Humidity Sensor Using Surface Adsorbed Channel Modulated GrapheneNanoribbon: NEGF Approach

Department of Electrical and Electronic Engineer
August 2014

Presented by-

ShifurRahmanShakil --------11121047
FatemaTuzZohra --------11121096
ParnaPramanik --------11121002
Raihanul Islam Tushar --------11121034

Table of Contents

Abstract

Flexible, highly sensitive and low cost humidity sensors are highly enviable in future generation sensor technology. As a result of recent year's research conducted concerning the applicability in gas and humidity sensors, graphene is reported to be an appropriate sensing material for this purpose. The inimitable structural, mechanical and electronic properties of graphene has attracted extensive attention of scientists, therefore the successful synthesis of novel two-dimensional (2D) graphene and the experimental observation of Dirac fermions in unpatterned graphene devices has been increasing rapidly. This thesis describes simulation based study of humidity sensing ability of patterned graphene adsorbing vapour (H_2O) and investigate electronic and quantum transport properties of these system such as Device Density of States (DDOS), Electrostatic Effective Potential (EDP), Conductivity (G) and Current-Voltage (I-V) characteristics. Transport simulation is based on Non-equilibrium Green's Function (NEGF) formalism. In our thesis, we have considered three cases such as semiconducting grapheme nanoribbon (N=10), metallic grapheme nanoribbon (N=11) and cascade hetero-graphene nanoribbon, where sensing medium is semiconducting GNR (N=10) and contact is metallic GNR (N=11) to realize the effect of H_2O adsorption on it. We have calculated the highest number of H_2O molecules that can be absorbed on corresponding to the area of GNR to get maximum current. Later on we propose a simple schematic model to characterize device performance which incorporates the effect of metal contact resistance with GNR.

Acknowledgement

We would like to start by acknowledging few people whose hard work and constant support made this thesis work possible. Firstly, we would like to express our deepest gratitude and sincere thanks to our thesis supervisor, Dr. Mohammed Belal Hossain Bhuian who constantly encouraged us. He has been very kind and would always like to discuss with us with great patience whenever we faced challenges and difficulties. Special regards to our thesis co-supervisor, Atanu Kumar Saha. He enabled us to develop the core concepts and basics for understanding this topic. Without his supervision, effective support and positive feedback we would not have been able to complete the thesis successfully. We all have worked extremely hard on the thesis as a team and hopefully our work will be appreciated by our supervisor.

Introduction

The discovery of a new material brings with it some of the most exciting and fruitful periods of scientific and technological research. With new materials come new opportunities to reexamine old problems as well as pose new ones. The recent discovery of graphene, atomically thin layers of graphite, has brought such a period. It is lighter than a feather, stronger than steel, yet incredibly flexible and more conductive than copper. It has been hailed as “the miracle material” as its possible uses are apparently almost endless. Andre Geim and Konstantin Novoselov at the University of Manchester won the Nobel Prize in Physics in 2010 "for groundbreaking experiments regarding the two-dimensional material graphene". For the first time, it is possible to isolate single two dimensional atomic layers of atoms. These are among the thinnest objects imaginable. The strongest bond in nature, the C-C bond covalently locks these atoms in place giving them remarkable mechanical properties. As an electronic material, graphene represents a new playground for electrons in 2, 1, and 0 dimensions where the rules are changed due to its linear band structure. Scattering is low in this material allowing for the observation of the Quantum Hall Effect (QHE), and the unique band structure of graphene gives this old effect a new twist.

In recent years, much attention has been focused on nanoelectronic devices [1-3] and molecular gas adsorption. Since gas and vapor adsorption by these systems could change their electronic properties, this property can be used as a gas and humidity sensing property. The previous and recent researchers have concentrated to focus on the interaction of small gas molecule, such as CO, NO_2 and NH_3 with the pristine graphene in theory [4] and CO_2 sensing using graphene sheet in experiment [5]. The interaction between small molecules and graphene can be highly enhanced by introducing adsorption into 2D nanosheets of graphene. Again, it can be shown that water (H_2O) molecules adsorbed on graphene cause defects in it which facilitate to electron-tunnelling of the band gap and cause widening of graphene band gap to 0.206 eV [6]. However, the changes in resistance are directly influenced by the amount of water vapour adsorbed by the graphene [7]. Electronic and transporting properties of these systems such as Device Density of States (DDOS), Electrostatic Effective Potential (EDP), Conductivity (G) and Current-Voltage (I-V) characteristics are greatly influenced by the adsorption of H2O.

We have considered three cases such as metallic graphene nanoribbon (N=11), semiconducting graphene nanoribbon (N=10) and cascade hetero-graphene nanoribbon, where sensing medium is semiconducting GNR (N=10) and contact is metallic GNR (N=11) to realize the effect of H_2O adsorption on it. In this work, we briefly outline a formalism that combines DFT with the Keldysh non-equilibrium Green's functions (NEGF) so that non-equilibrium quantum transport properties can be predicted from atomistic approach without any phenomenological parameters [8-9]. We have made transport simulation is based on Non-equilibrium Green's Function (NEGF) formalism

Chapter 1: Significance of Graphene:

1.1 Basic concept:

Graphene is pure two dimensional allotrope of carbon in the form of a very thin, nearly transparent sheet, one atom thick. It is remarkably strong for its very low weight and conducts heat and electricity with great efficiency and it can be wrapped up into 0D Bucky balls, rolled into 1D nanotube or stacked into 3D graphite (shown in figure 1). Because it is virtually two-dimensional, it interacts oddly with light and with other materials Researchers have identified the bipolar transistor effect, ballistic transport of charges and large quantum oscillations.

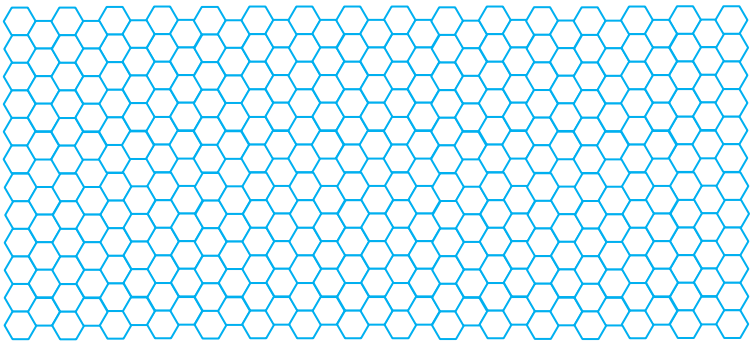

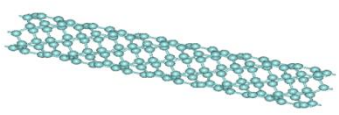

Fig. 1 Graphene is a 2D building material for carbon materials of all other dimensionalities. [1]

Technically, 7 -graphene is a crystalline allotrope of carbon with 2-dimensional properties. It can be described as a one-atom thick layer of graphite. It is the basic structural element of other allotropes, including graphite, charcoal, carbon nanotubes and fullerenes. Graphene can also be considered as an indefinitely large aromatic molecule, the limiting case of the family of flat polycyclic aromatic hydrocarbons.

Graphene research has expanded quickly since the substance was first isolated in 2004. Research was informed by theoretical descriptions of graphene's composition, structure and properties, which had all been calculated decades earlier. High-quality graphene also proved to be surprisingly easy to isolate, making more research possible.

1.2 Graphene nanoribbons:

Graphene nanoribbons, GNRs, are strips of graphene with ultra-thin width less than 50 nm. The calculations based on tight binding theory predicts that its electronic states mostly depend on their width and edge structures – armchair or zigzag, which shows that armchairs can be either metallic or semiconducting while zigzags are always metallic, depending on their width. Zigzag edges provide the edge localized state with non-bonding molecular orbital near the Fermi energy and thus additional energy states appear on their edges. This makes all the zigzag GNRs metallic. Again calculations based on Discrete Fourier Transforms (DFT) show that armchair nanoribbons are semiconducting with an energy gap scaling with the inverse of the GNR width[1]. Research showed that decreasing GNR width increases energy band gaps [8].

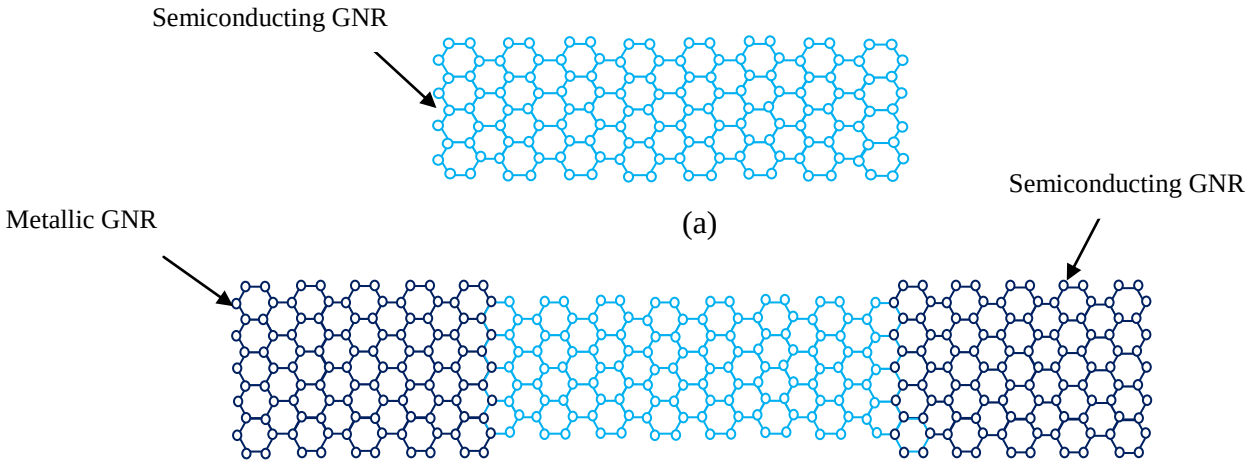

(a)

(b)

Fig. 2different types of GNR (a) semiconducting GNR (b) metallic and semiconducting cascaded GNR.

1.3 Properties:

1.3.1 Structural

Graphene's stability is due to a tightly packed, periodic array of carbon atoms and an sp2 orbital hybridization - a combination of orbital p_x and p_y that constitute the σ-bond. Graphene has three σ-bonds and one π-bond. The final p_z electron makes up the π-bond, and is key to the half-filled band that permits free-moving electrons.

Graphene sheets in solid form usually show evidence in diffraction for graphite's layering. This is true of some single-walled nanostructures. Transmission electron microscopy (TEM) studies show faceting at defects in flat graphene sheets and suggest a role for two-dimensional crystallization from a melt.

Graphene can self-repair holes in its sheets, when exposed to molecules containing carbon, such as hydrocarbons. Bombarded with pure carbon atoms, the atoms perfectly align into hexagons, completely filling the holes.

The atomic structure of isolated, single-layer graphene was studied by TEM on sheets of graphene suspended between bars of a metallic grid. Electron diffraction patterns showed the expected honeycomb lattice. Suspended graphene also showed "rippling" of the flat sheet, with amplitude of about one nanometer. These ripples may be intrinsic to the material as a result of the instability of two-dimensional crystal. Atomic resolution real-space images of isolated, single-layer graphene on SiO2 substrates are available via scanning tunneling microscopy. Rippling on SiO2 is caused by conformation of graphene to the underlying SiO2, and is not intrinsic.

1.3.2 Band Structure of Graphene:

Graphene - a monolayer of carbon atoms packed into a honeycomb lattice, is one of the most intriguing systems in Solid State physics today. Each carbon atom in the honeycomb lattice is surrounded by three neighbors, with which it shares electrons. Three out of four valence electrons form the chemical bonds, and form a relatively low-

lying band. The one, which is left, has a character of a p_z-orbital, perpendicular to the graphene plane.

The most popular description of graphene band structure is the tight binding one, first done by Wallace. The band structure exhibits very unique features: the conduction and the valence bands are not separated by a gap, and do not overlap either. Since the effective masses are given by the curvature of the energy bands, this corresponds to zero effective mass. The connection points of the cones are called the Dirac points in the first Brillouin zone. The electron dispersion in the vicinity of the Dirac points is conical and not parabolic, as in most semiconductors. Hence, the group velocity $v_g = E(\mathrm{k})$ is independent of the energy. The Fermi level for undoped graphene lies exactly at the intersection points, and graphene is a gapless semiconductor. Since the dispersion curve resembles that of ultra-relativistic particles, one can write a relativistic dynamic equation for the excitations. Such equation can be derived from the tight binding model, and the resulting equation is in fact the well-known Dirac equation for mass less particles.

1.3.3 Electronic:

One of the most useful properties of graphene is that it is a zero-overlap semimetal (with both holes and electrons as charge carriers) with very high electrical conductivity. Carbon atoms have a total of 6 electrons; 2 in the inner shell and 4 in the outer shell. The 4 outer shell electrons in an individual carbon atom are available for chemical bonding, but in graphene, each atom is connected to 3 other carbon atoms on the two dimensional plane, leaving 1 electron freely available in the third dimension for electronic conduction. These highly-mobile electrons are called π-electrons and are located above and below the graphene sheet. These π-orbital overlap and help to enhance the carbon to carbon bonds in graphene. Fundamentally, the electronic properties of graphene are dictated by the bonding and anti-bonding (the valance and conduction bands) of these pi orbital.

Research has proved that at the Dirac point in graphene, electrons and holes have zero effective mass. This occurs because the energy – movement relation (the spectrum for excitations) is linear for low energies near the 6 individual corners of the Brillouin zone. These electrons and holes are known as Dirac fermions, or Graphinos, and the 6 corners of the Brillouin zone are known as the Dirac points. Due to the zero density of states at the Dirac points, electronic conductivity is actually quite low. However, the

Fermi level can be changed by doping (with electrons or holes) to create a material that is potentially better at conducting electricity than, for example, copper at room temperature.

Tests have shown that the electronic mobility of graphene is very high, above 15,000 $cm2 \cdot V{-}1 \cdot s{-}1$ and theoretically potential limits of 200,000 $cm2 \cdot V{-}1 \cdot s{-}1$ (limited by the scattering of graphene's acoustic photons). It is said that graphene electrons act very much like photons in their mobility due to their lack of mass. These charge carriers are able to travel sub-micrometer distances without scattering; a phenomenon known as ballistic transport. With silicon dioxide as the substrate, for example, mobility is potentially limited to 40,000 $cm2 \cdot V{-}1 \cdot s{-}1$.

1.3.4 Mechanical strength:

As a single, virtually defect-free crystal, graphene is predicted to have an intrinsic tensile strength higher than any other known materials and tensile stiffness similar to graphite. Due to the strength of its 0.142 Nm-long carbon bonds, graphene is the strongest material ever discovered, with an ultimate tensile strength 130 GPa, compared to 0.4GPa for steel. Not only is graphene extraordinarily strong, it is also very light at 0.77milligrams per square meter.

What makes this particularly special is that graphene also contains elastic properties, being able to retain its initial size after strain. By creating holes within a sheet of graphene, then "doping" those holes with desired impurities, semiconductors can be made that are nearly unbreakable and highly flexible. In 2007, Atomic force microscopic (AFM) tests were carried out on graphene sheets that were suspended over silicon dioxide cavities. These tests showed that graphene sheets (with thicknesses of between 2 and 8 Nm) had spring constants in the region of 1-5 N/m and a Young's modulus of 0.5 TPa where diamond has 1221 GPa.

1.3.5 Optical:

Graphene's ability to absorb a rather large 2.3% of white light is also a unique and interesting property, especially considering that it is only 1 atom thick. This is due to its aforementioned electronic properties; the electrons acting like mass less charge carriers with very high mobility. Adding another layer of graphene increases the amount of white

light absorbed by approximately the same value (2.3%). Graphene's opacity of $\pi\alpha \approx$ 2.3% equates to a universal dynamic conductivity value of $G=e2/4\hbar$ (±3%) over the visible frequency range.

Because of these impressive characteristics graphene has a unique absorption when the input optical intensity is above a threshold value. This nonlinear optical behavior is termed saturable absorption and the threshold value is called the saturation fluence. Graphene can be saturated readily under strong excitation over the visible to near-infrared region, due to the universal optical absorption and zero band gap. This has relevance for the mode locking of fiber lasers, where full band mode locking has been achieved by graphene-based saturable absorber. Due to this special property, graphene has wide application in ultrafast photonics. Moreover, the optical response of graphene layers can be tuned electrically. Saturable absorption in graphene could occur at the Microwave and Terahertz band, owing to its wideband optical absorption property. The microwave saturable absorption in graphene demonstrates the possibility of graphene microwave and terahertz photonics devices, such as microwave saturable absorber, modulator, polarizer, microwave signal processing and broad-band wireless access networks.

1.3.6 Thermal:

Graphene is a perfect thermal conductor. Its thermal conductivity was measured recently at room temperature and it is much higher than the value observed in all the other carbon structures as carbon nanotubes (CNR), graphite and diamond (greater than 5000 $W \cdot m^{-1} \cdot K^{-1}$). The ballistic thermal conductance of graphene is isotropic, i.e. same in all directions. Graphite, the 3 D version of graphene, shows a thermal conductivity about 5 times smaller (1000 $W \cdot m^{-1} \cdot K^{-1}$). The phenomenon is governed by the presence of elastic waves propagating in the graphene lattice, called phonons. The studies of thermal conductivity in graphene have important implications in graphene-based electronic devices. Even on a substrate, thermal conductivity reaches 600 $W \cdot m^{-1} \cdot K^{-1}$.

Graphene is said to be the least stable structure until about 6000 atoms. Because of this property a graphene sheet is thermodynamically unstable if its size is less than about 20nm and becomes most stable fullerene only for molecules larger than 24,000 atoms.

The near-room temperature thermal conductivity of graphene was measured to be between (4.84±0.44) × 10^3 to (5.30±0.48) × 10^3 $W \cdot m^{-1} \cdot K^{-1}$. These measurements, made by a non-contact optical technique, are in excess of those measured for carbon nanotubes or diamonds. The isotopic composition, the ratio of ^{12}C to ^{13}C,has a significant impact on thermal conductivity, where isotopically pure ^{12}C graphene has higher conductivity than either a 50:50 isotope ratio or the naturally occurring 99:1 ratio. It can be shown by using the Wiedemann–Franz law, that the thermal conduction is phonon-dominated. However, for a gated graphene strip, an applied gate bias causing a Fermi energy shift much larger than $k_B T$ can cause the electronic contribution to increase and dominate over the phonon contribution at low temperatures. The ballistic thermal conductance of graphene is isotropic.

Potential for this high conductivity can be seen by considering graphite, a 3D version of graphene that has basal plane thermal conductivity of over a 1000 $W \cdot m^{-1} \cdot K^{-1}$. In graphite, the c-axis (out of plane) thermal conductivity is over a factor of ~100 smaller due to the weak binding forces between basal planes as well as the larger lattice spacing.

Considering the lattice vibrational modes (phonons) of the material, graphene unit cellcontainsN=2 carbon atoms. This leads to the formation of three acoustic (A) and three optical (O) phonon modes, with the dispersions. The dispersion is the relationship between the phonon energyEor frequency ω ($E = \hbar\omega$, where$\hbar$ is the reduced Planck constant) and the phonon wave vector q. Longitudinal (L) modes correspond to atomic displacements along the wave propagation direction (compressive waves), whereas transverse (T) modes correspond to in-plane displacements perpendicular to the propagation direction (shear waves). In typical three-dimensional (3D) solids, transverse modes can have two equivalent polarizations, but the unique 2D nature of graphene allows out-of-plane atomic displacements, also known as flexural (Z) phonons.At low q near the center of the Brillouin zone, the frequencies of the transverse acoustic (TA) and longitudinal acoustic (LA) modes have linear dispersions of$\omega_{TA} \sim V_{TA} q$ and $\omega_{TA} \sim V_{TA} q$, respectively. The group velocities V_{TA}~ 13.6 km/s and V_{TA} ~ 21.3 km/s are four to six times higher than those in silicon or germanium because of the strong in-plane sp^2 bonds of graphene and the small mass of carbon atoms. In contrast, the flexural ZA modes have an approximately quadratic dispersion,$\omega_{TA} \sim aq^2$,, where a ~

6.2 x 10^{-7} m^2/s. These ZA modes are responsible for many of the unusual thermal properties of graphene.

1.4 Applications and Uses:

Lower cost of display screens in mobile devices: Researchers have found that graphene can replace indium-based electrodes in organic light emitting diodes (OLED). These diodes are used in electronic device display screens which require low power consumption. The use of graphene instead of indium not only reduces the cost but eliminates the use of metals in the OLED, which may make devices easier to recycle.

Lithium-ion batteries that recharge faster: These batteries use graphene on the surface of the anode. Defects in the graphene sheet (introduced using a heat treatment) provide pathways for the lithium ions to attach to the anode substrate. Studies have shown that the time needed to recharge a battery using the grapheme anode is much shorter than with conventional lithium-ion batteries.

Ultra-capacitors with better performance than batteries: These ultra-capacitors store electrons on graphene sheets, taking advantage of the large surface of graphene to provide increase the electrical power that can be stored in the capacitor. Researchers are projecting that these ultra-capacitors will have as much electrical storage capacity as lithium ion batteries but will be able to be recharged in minutes instead of hours.

Components with higher strength to weight ratios: Researchers have found that adding graphene to epoxy composites may result in stronger/stiffer components than epoxy composites using a similar weight of carbon nanotubes. Graphene appears to bond better to the polymers in the epoxy, allowing a more effective coupling of the graphene into the structure of the composite. This property could result in the manufacture of components with high strength to weight ratio for such uses as windmill blades or aircraft components.

Storing H_2 for fuel cell powered cars: Researchers have prepared graphene layers to increase the binding energy of hydrogen to the graphene surface in a fuel tank, resulting in a higher amount of hydrogen storage and therefore a lighter weight fuel tank. This could help in the development of practical hydrogen fueled cars.

Lower cost fuel cells: Researchers have demonstrated how to produce edge-halogenated graphene nanoplatelets that have good catalytic properties. They prepared the nanoplatelets by ball-milling graphene flakes in the presence of chlorine, bromine or iodine. They believe these halogenated nanoplatelets could be used as a replacement for expensive platinum catalytic material in fuel cells.

Low cost water desalination: Researchers have determined that graphene with holes the size of a nanometer or less can be used to remove ions from water. They believe this can be used to desalinate sea water at a lower cost than the reverse osmosis techniques currently in use.

Lightweight natural gas tanks: Researchers have developed a composite material using plastic and graphene nanoribbons that block the passage of gas molecules. This material may be used in applications ranging from soft drink bottles to lightweight natural gas tanks.

More efficient dye sensitized solar cells: A honeycomb like structure of graphene has been developed in which the graphene sheets are held apart by lithium carbonate. They have used this "3D graphene" to replace the platinum in a dye sensitized solar cell and achieved 7.8 percent conversion of sunlight to electricity.

Electrodes with very high surface area and very low electrical resistance: Researchers at Rice University have developed electrodes made from carbon nanotubes grown on graphene. The researchers first grow graphene on a metal substrate then grow carbon nanotubes on the graphene sheet. Because the base of each nanotube is bonded, atom to atom, to the graphene sheet the nanotube-graphene structure is essentially one molecule with a huge surface area.

Lower cost solar cells: A solar cell has been built that uses graphene as a electrode while using bucky balls and carbon nanotubes to absorb light and generate electrons; making a solar cell composed only of carbon. The intention is to eliminate the need for higher cost materials, and complicated manufacturing techniques needed for conventional solar cells.

Transistors that operate at higher frequency: The ability to build high frequency transistors with graphene is possible because of the higher speed at which electrons in graphene move compared to electrons in silicon. Researchers are also developing lithography techniques that can be used to fabricate integrated circuits based on graphene.

Sensors to diagnose diseases: These sensors are based upon graphene's large surface area and the fact that molecules that are sensitive to particular diseases can attach to the carbon atoms in graphene. For example, researchers have found that graphene, strands of DNA, and fluorescent molecules can be combined to diagnose diseases. A sensor is formed by attaching fluorescent molecules to single strand DNA and then attaching the DNA to graphene. When an identical single strand DNA combines with the strand on the graphene, a double strand DNA formed floats off from the graphene, increasing the fluorescence level. This method results in a sensor that can detect the same DNA for a particular disease in a sample.

Chemical sensors effective at detecting explosives: These sensors contain sheets of graphene in the form of a foam which changes resistance when low levels of vapors from chemicals, such as ammonia, is present.

Chapter 2: Previous work based on GNR sensor:

Measurement and control of environmental humidity is one of the most important issues that have emerged in recent years in industrial, agricultural and human activities. Various types of humidity sensors have been developed over the course of many years in the recent past. To meet the growing needs of people humidity sensors having higher sensitivity, wider detection range as well as quicker response and shorter recovery times are being manufactured each passing moment. For the achievement of these goals, considerable attention has been rendered towards the development of humidity sensitive materials or elements, especially Nanomaterials due to their high surface to volume ratio. Many materials have been investigated including one dimensional (1D) carbon, silicon, ceramic nanomaterials, semiconductor nanoparticles and metal oxide nanowires and nanofilms. Using these materials the progress remains limited to the day.

However graphene is a material that is a novel humidity sensing material that possesses high and even sensitivity for the full range of humidity. Graphene is two-dimensional monolayer of sp^2-bonded carbon atoms exhibiting exceptional mechanical, thermal and electrical properties. It holds great potential for ultrasensitive detection and sensors based on graphene have raised significant interest. These sensors show very high sensitivity to gases including NO_2, NH_3 and so on. Further, sensors with single –molecule sensitivity have also been reported.

In recent years many works have been published concerning the applicability of graphene in gas sensors with an emphasis on the sensitivity, selectivity and stability of graphene sensors in artificial conditions. In one insightful work Electrical Conductivity of Hydrogenated Armchair Nanoribbon as a Gas Sensor Using Non-Equilibrium Green's Function Method was done with very promising results. The armchair graphene nanoribbons (AGNR) are focused on in this work which is hydrogenated from their edges which are then called hydrogenated AGNR (HAGNR). Here a HAGNR has been considered where hydrogen or oxygen molecules were absorbed on its surface. The results show that at low adsorption concentrations, more adsorption of hydrogen or oxygen molecules leads to the increase of conductivity of the system, while at high adsorption concentrations, more adsorption leads to the reduction of conductivity. Therefore, conductivity could identify the percentage of adsorbed gas molecules.

In the clean HAGNR the upper (lower) edge sites construct metallic regions separated by semiconducting regions. Adsorption of hydrogen/oxygen molecule by metallic sites leads to a reduction of current, while those by semiconducting sites lead to an increase in current. The adsorption of hydrogen/oxygen by semiconducting sites converts these sites to metallic sites. Hence these adsorption increases current while the adsorption of hydrogen/oxygen by metallic sites reduces the current.

It was also discovered that at high adsorption concentrations, adsorption by semiconducting sites with bigger energy gap increases current more than smaller energy gap semiconductor sites, and adsorption by more metallic sites decreases current with respect to those sites with low metallic features.

Hence in this study a lot of facts about graphene came to the light which enables it to be used as a gas sensor with a lot of precision. Using the NEGF method effects of gas adsorption on the electronic properties of HAGNR was investigated in this paper. It was found that at low adsorption concentration, adsorption by metallic HAGNR sites decreases current, while adsorption by semiconducting HAGNR sites increases current. On the other hand, at high adsorption concentration, the whole system becomes metallic, so by increasing adsorption concentration, current always decreases. Also at low adsorption the conductivity of the system increases by increasing adsorption, while at high adsorptions, the conductivity decreases by increasing adsorption.

Another such example where graphene has been exploited as a sensor is in Civil Engineering where a Graphene-Based Resistive Humidity Sensor for In-Situ Monitoring of Drying Shrinkage and Intrinsic Permeability in Concrete has been proposed. Here relevance and feasibility of embedding relative humidity nanosensors within concrete has been discussed. The localized and continuous knowledge of relative humidity within a concrete structure could provide useful insights into drying shrinkage. It could also improve the measurement of the intrinsic permeability leading to the correct assessment of structural durability. Here a low-cost down scalable resistive device made of a 10 nm graphene sheet grown directly on glass has been proposed atop which are ink-jet printed silver electrodes. The device resistance increases significantly with relative humidity (RH), especially above 40% RH.

Drying shrinkage is responsible for significant degradations of concrete materials and it depends strongly on both capillary pressure and liquid water saturation. Denoting $\mathcal{E}$ as the drying shrinkage the relationship is as follows:

$$d\mathcal{E} = \frac{bS}{K}\, dp = -\frac{bpRT}{KM}\, S\, \frac{dh}{h}$$

Where *b* is the Biot's coefficient and *K* is the bulk modulus of the drained material. If the relative humidity repartition *h(x,t)*from the embedded sensors are known then using the above equation and an integration step can be used to yield the total shrinkage. Previously the external relative humidity was used to determine the drying shrinkage but with the help of this device a more accurate measure is possible of the relative humidity

inside the concrete which allows a more precise measure of the durability of the concrete. Also with this device a continuous measurement of shrinkage is achieved and consequently an improved prediction of shrinkage related cracking is attainable.

The device proposed here is composed of glass substrate covered by few-layer-graphene with silver electrodes on top. It is robust since it will be inside a harsh material. Also the device is small in order to minimize perturbation of the medium. CH_4/H_2 PECVD (Plasma Enhanced Chemical Vapor Deposition) process enables graphene growth on a glass substrate heated at 450^oC. A continuous sheet of few layer graphene grows directly at the interface between a 200 nm catalytic Nickel layer and the glass substrate. Silver electrodes are installed by ink-jet printing using INKTEC TEC-IJ-010 silver ink in a Dimatix DMP-2800 materials printer of size 10 μm^2.

For finding the resistive behavior of the device two neighboring electrodes are contacted by microtips and the I-V characteristic is acquired using a MATLAB controlled Keithley 2612 Source Meter. The I-V characteristic is linear showing ohmic behavior of the device. The resistance is then deducted by least-square fitting the curve. For different graphene sheet thicknesses the resistances differ at 45% RH. After that the device is put to the test by changing the RH by an amount of 5% steps and calculating the resistance at every 4 seconds interval. Two such devices were implemented and for the both of them the sensitivity to humidity is clear, especially above 40% RH. For the 2.2 kΩ device the resistance increases by 80 Ω (4%) between 45% and 85%; for the 15 kΩ device the resistance increases by 480 Ω (3%) between 5% and 65%. As seen from the results it is clear that although relative resistance variations are small, absolute resistance variations appear large enough to be measured by discrete electronic components.

In another work the Influence of Humidity on the Resistance Structures with Graphene Sensor Layer has been studied and analysed. Fluctuations of the content of steam in air and the unknown ability to absorb it by a sensor layer are the most interfering factor in the actual operation of devices for detecting gases in the atmosphere. In this work the Density Functional Theory (DFT) analysis it has been used to show that water molecules

absorbed on graphene causes defect in it which facilitates to electrons tunneling of the bandgap and cause widening of bandgap in graphene.

Graphene is a hydrophilic material and so when water is absorbed on its surface, the structure behaves like a semiconductor which causes the width of its bandgap to increase. Therefore, the graphene swells and shrinks in relation to the relative humidity level. It is believed that this swelling and shrinking is the cause of resistance changes observed at various humidity levels.

Experiments were carried out to investigate the sensitivity of graphene affected by nitrogen dioxide (NO_2). At first, the reaction of the sensor structure with graphene on the action of moist air (5.7% humidity at 50^oC temperature) is carried out and then NO_2 gas was introduced at intervals. It was observed that resistance remained constant (about 11.5Ω) when only air flows through the channel and decreases when NO_2 passes through it. The structure does not regain its previous resistance after the first reaction with NO_2. This is because when molecules of NO_2 gases are absorbed onto graphene, as bringing electrons from graphene holes are created which decreases resistance. The decreased resistance is constant and does not fade entirely after gas exchange because adsorption of NO_2 into graphene structure is constant. Part of NO_2 reacts with the absorbed water forming nitric acid which generates stable defects in graphene structure.

The same experiment was carried out with decreased amount of humidity (4.78%) in air. The response of the sensing structure is faster than the previous experiment and showed a clear decrease in resistance. When temperature was increased to 120^oC and other factors remaining the same, it showed a slide increase in resistance. This increase is greater when percentage of humidity is increased in air.

The Ultrahigh Humidity Sensitivity of Graphene Oxide was studied in another work. Humidity sensors have been extensively used in various fields and numerous problems are encountered when using humidity sensors, including low sensitivity, long response and recovery times, and narrow humidity detection ranges. For these reasons using graphene oxide (G-O) films as humidity sensing materials are adapted in this particular paper for its improved sensitivity compared to conventional sensors (about 10 times

better). Moreover, G-O based sensors have faster response time (less than ¼ of that of the conventional one) and recovery time (less than ½ of that of the conventional one) which makes it a favorable choice of material in many applications.

The sensitivity of the water can be increased by the fact that the basal plane and edges of G-O platelets are composed of distributed chemical groups containing oxygen. Moreover, the chemical groups can make G-O electrically insulating, which enables the convenient incorporation of graphene oxide into capacitive sensors.

The humidity sensitivity of G-O based sensors reach up to 37800% at 15%–95% relative humidity (RH). On the other hand, conventional capacitive humidity sensors have sensitivities ranging from 43% to 2900%. The response time of G-O based humidity sensors are 10.5 s which is 1/120 to ¼ that of conventional humidity sensors. The sensors also exhibit high sensitivity (16067%) which is 133 to 277 times higher than that of conventional humidity sensors even under low humidity conditions (<40%RH).

The dependence of the sensor capacitance on RH at different frequencies (100 Hz, 1 kHz and 10 kHz) was invested at 25^{o}C. As the RH level increases, the output capacitance of the sensor shifts higher monotonically. Absorbed water can increase the dielectric constant and the capacitance. Among the three frequencies, 100 Hz exhibits the best linearity. The sensor activity is then defined quantitatively as follows:

$$\text{Sensitivity} = (C_x - C_{15})/C_{15} \qquad (1)$$

$$\text{Sensitivity} = (C_x - C_{15})/ (RH_x - RH_{15})$$

where C_x and C_{15} are the capacitances at x% and 15% RH levels respectively. It is also observed that the capacitance decreases with increasing frequency. Hence the capacitance became independent of the humidity with increasing frequency. This is because at low frequencies the electric field direction changes slowly, while at high frequencies the electric field direction changes so fast that the polarization of the absorbed water cannot catch up with it and hence the dielectric constant is small and independent of RH.

After that the relationship between the sensitivity defined in equation (1) and RH was investigated. It was observed that the sensitivity at 1 kHz is higher than the other two frequencies. Further, when the RH level changes from 15% RH to 95% RH, the capacitance rises from 9.8 pF to 3710 pF and the corresponding relative capacitance change is 37800%. Therefore, 100 Hz and 1 kHz were selected as the operating frequencies in the experiments.

For checking the stability of the humidity sensor, it was repeatedly tested under fixed humidity levels (15%, 35%, 55%, 75% and 95% RH) over a period of 30 days. The capacitance variation is less than 4% at each humidity region for one month at 100 Hz and less than 6% at each humidity region for one month at 1 kHz. Hence the sensor proved to be very stable.

The response and recovery times of the sensors were also very promising. The sensor response time (humidification from 23% RH to 86% RH) was about 10.5 s, and the recovery time (desiccation from 86% RH to 23% RH) was about 41 s. These excellent response and recovery times are not only ascribed to the abundant hydrophilic functional groups on G-O sheets, but also to the large interlayer space in the G-O films which facilitates water adsorption and desorption.

Chapter 3: NEGF and DFT:

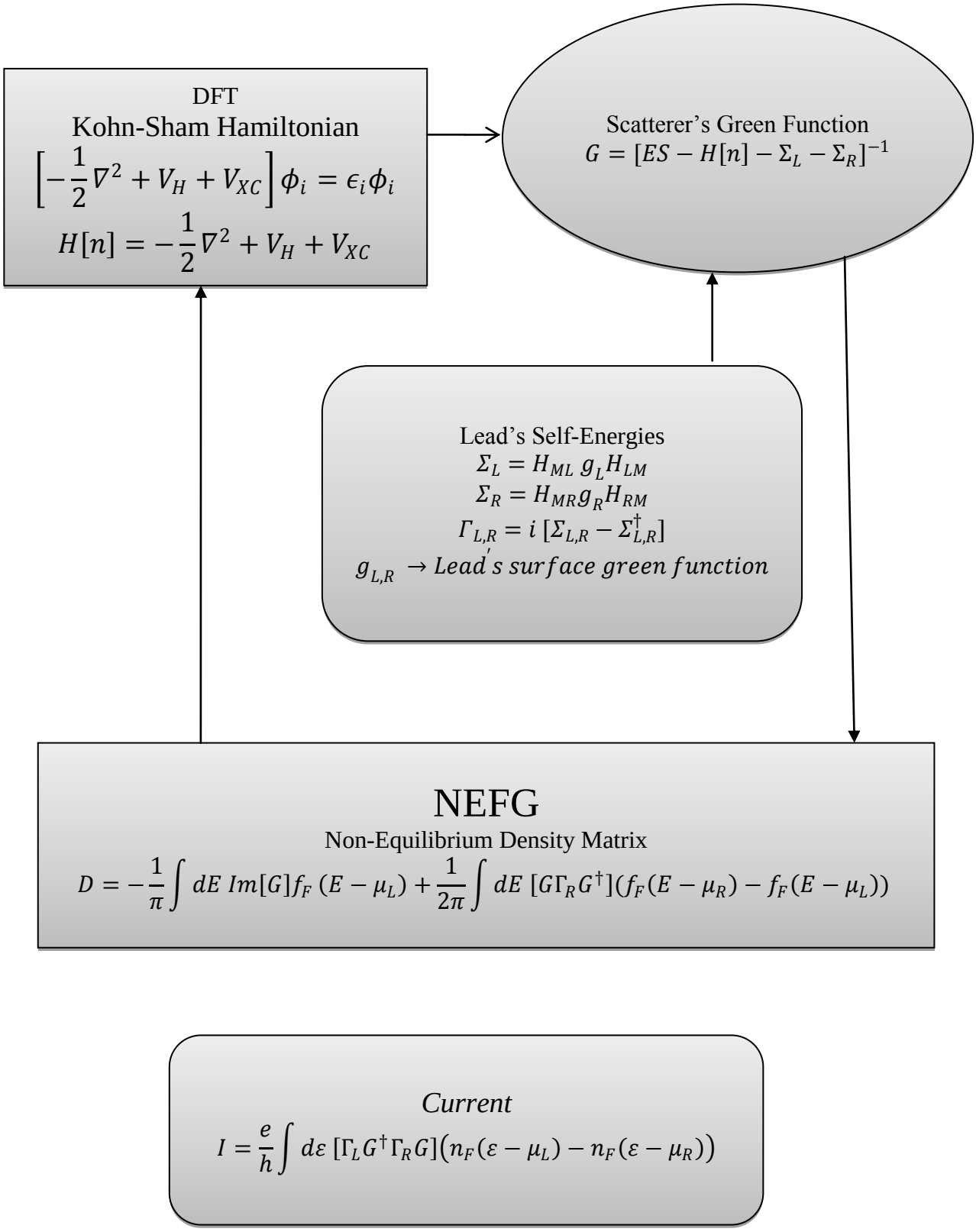

3.1 The Density Functional Theory (DFT):

The density functional theory (DFT) is presently the most successful approach to compute the electronic structure of matter. Its capability ranges from atoms, molecules and solids to nuclei and quantum and classical fluids. In its original formulation, DFT provides the ground state properties of a system and the electron density plays a key role. For example DFT predicts a great variety of molecular properties: molecular structures, vibrational frequencies, atomization energies, ionization energies, electric and magnetic properties, reaction paths, etc. The original density functional theory has been generalized to deal with many different situations: spin polarized systems, multicomponent systems such as nuclei and electron hole droplets, free energy at finite temperatures, superconductors with electronic pairing mechanisms, relativistic electrons, time-dependent phenomena and excited states, bosons, molecular dynamics, etc.

The ultimate goal of most approaches in solid state physics is the solution of the time-independent, non-relativistic Schrodinger equation:

$$H\psi_i(x_1 x_2 \dots x_N R_1 R_2 \dots R_M) = E_i \psi_i(x_1 x_2 \dots x_N R_1 R_2 \dots R_M)$$

H is the Hamiltonian for a system consisting of M nuclei and N electrons.

$$H = -\frac{1}{2}\sum_{i=1}^{N}\nabla_i^2 - \frac{1}{2}\sum_{A=1}^{M}\frac{1}{M_A}\nabla_A^2 - \sum_{i=1}^{N}\sum_{A=1}^{M}\frac{Z_A}{r_{iA}} + \sum_{i=1}^{N}\sum_{j>i}^{N}\frac{1}{r_{ij}} + \sum_{A=1}^{M}\sum_{B>A}^{M}\frac{Z_A Z_B}{R_{AB}}$$

Here, A and B run over the M nuclei while i and j denote the N electrons in the system. The first two terms describe the kinetic energy of the electrons and nuclei. The other three terms represent the attractive electrostatic interaction between the nuclei and the electrons and repulsive potential due to the electron-electron and nucleus-nucleus interactions.

3.1.1 Born-Oppenheimer approximation:

Due to their masses the nuclei move much slower than the electrons we can consider the electrons as moving in the field of fixed nuclei, the nuclear kinetic energy is zero and their potential energy is merely a constant. Thus, the electronic Hamiltonian reduces to:

$$H_{elec} = -\frac{1}{2}\sum_{i=1}^{N}\nabla_i^2 - \sum_{i=1}^{N}\sum_{A=1}^{M}\frac{Z_A}{r_{iA}} + \sum_{i=1}^{N}\sum_{j>i}^{N}\frac{1}{r_{ij}} = T + V_{Ne} + V_{ee}$$

The solution of the Schrodinger equation with H_{elec} is the electronic wave function ψ_{elec} and the electronic energy E_{elec}. The total energy E_{tot} is then the sum of E_{elec} and the constant nuclear repulsion term E_{nuc}.

$$H_{elec}\,\psi_{elec} = E_{elec}\,\psi_{elec}$$

$$E_{tot} = E_{elec} + E_{nuc} \text{ where} E_{nuc} = \sum_{A=1}^{M}\sum_{B>A}^{M}\frac{Z_A Z_B}{R_{AB}}$$

3.1.2 The Electron Density:

The electron density is the central quantity in DFT. It is defined as the integral over the spin coordinates of all electrons and over all but one of the spatial variables:

$$\rho(\vec{r}) = N\int \dots \int \psi\,(\overrightarrow{x_1}, \overrightarrow{x_2}, \dots, \overrightarrow{x_N})^2\, dx_1 \overrightarrow{dx_2}, \dots, \overrightarrow{dx_N}$$

$\rho(\vec{r})$ determines the probability of finding any of the N electrons within volume element $\overrightarrow{dr}$. $\rho(\vec{r})$is a non-negative function of only the three spatial variables which vanishes at infinity and integrates to the total number of electrons.

3.1.3 The First Hohenberg-Kohn Theorem:

The first Hohenberg-Kohn theorem demonstrates that the electron density uniquely determines the Hamiltonian operator and thus all the properties of the system. This first theorem states that the external potential $V_{ext}(r)$ is (to within a constant) a unique functional of $\rho(r)$; since, in turn $V_{ext}(r)$ fixes H we see that the full many particle ground state is a unique functional of $\rho(r)$.

$\rho(r)$ determines N and $V_{ext}(r)$ and hence all the properties of the ground state, for example the kinetic energy T[ρ], the potential energy V [ρ], and the total energy E[ρ]. Now, we can write the total energy as:

$$E[\rho] = E_{Ne}[\rho] + T[\rho] + E_{ee}[\rho] = \int \rho(r)\, V_{Ne}(r) dr + F_{HK}[\rho]$$

$$F_{HK}[\rho] = T[\rho] + E_{ee}$$

This functional $F_{HK}[\rho]$ is the basis of density functional theory. If it were known we would have solved the Schrodinger equation exactly! And, since it is a universal functional completely independent of the system at hand, it applies equally well to the hydrogen atom as to gigantic molecules such as, say, DNA! $F_{HK}[\rho]$ contains the functional for the kinetic energy T[ρ] and that for the electron-electron interaction, $E_{ee}[\rho]$.

3.1.4 Calculations of Different Parameters:

The Electrical Current:

$$I = \frac{2e}{h} \int_{-\infty}^{\infty} d\varepsilon \; Tr\{tt^{\dagger}\} \left[f\left(\varepsilon - \frac{eV}{2}\right) - f\left(\varepsilon + \frac{eV}{2}\right) \right]$$

The Device Density of States (DDOS):

$$DDOS(E) = \frac{1}{2\pi} Tr\left[G^R\left(\Gamma^L + \Gamma^R\right)G^A\right]$$

Conductance (G):

$$G(E) - \frac{2q^2}{h} Tr[\Gamma^L G^R \Gamma^R G^A]$$

Electrostatic Difference Potential (EDP):

$$EDP\left(\frac{r}{\max(r)}\right) = \frac{U(r) - \max\big(U(r)\big)}{\max(U(r))}$$

Where, U(r) is the electrostatic potential calculated from Poisson's equation using finite difference algorithm and r represents two dimensional space coordinates (x,y,z). EDP an unit less and normalized parameter. $G^R$is the Retarded Green's function where S and H are overlap integral matrix and device Hamilton matrix respectively. Tr represents Trace of matrix and $\Gamma^L = i\left[\Sigma_L - \Sigma_L^\dagger\right]$ and $\Gamma^R = i\left[\Sigma_R - \Sigma_R^\dagger\right]$ and $\Sigma^L(E)$ and $\Sigma^R(E)$ are the self-energy terms for left electrode and right electrode respectively.

3.2 The Nonequilibrium Green's Function (NEGF) Method:

For nanoscale systems the Landauer Formula is widely used for calculating the current:

$$I = \frac{2q}{h}\int_{-\infty}^{+\infty} T(E)[f(E-\mu_1) - f(E-\mu_2)]\,dE$$

Here T (E) is the transmission coefficient, f (E) is the Fermi-Dirac distribution function and μ_1 and μ_2 are the Fermi energies of the left and right contact of the conductor.
At the simplest case the thermal broadening function is given by the following equation which will be used in the calculation of conductance of graphene nanoribbons:

$$G(E) = \frac{2q^2}{h}\,T(E)$$

The Nonequilibrium Green's Function (NEGF) is a convenient method for calculating the transmission coefficient. The electron density was given by the electron density matrix. The density matrix is divided into left and right contributions:

$$D = D^L + D^R$$

The left density matrix contribution can be given from NEGF theory as follows:

$$D^L = \int \rho^L(\varepsilon)\, f\left(\frac{\varepsilon - \mu_L}{k_B T_L}\right)\, d\varepsilon$$

$$\rho^L(\varepsilon) = \frac{1}{2\pi} G(\varepsilon)\Gamma^L(\varepsilon)G^\dagger(\varepsilon)$$

Where $\rho^L(\varepsilon)$ in the above equation is the spectral density matrix. While there is a Nonequilibrium electron distribution in the central region, the electron distribution in the electrode is described by a Fermi function *f* with an electron temperature T_L.
The G(ε) is the retarded Green's function and Γ^L is the broadening function of the left electrode, given in terms of the left electrode self-energy as shown below:

$$\Gamma^L = \frac{1}{i}(\Sigma^L - (\Sigma^L)^\dagger)$$

A similar equation exists for the right density matrix contribution.

3.2.1 The Retarded Green's Function:

The retarded Green's function matrix is a key quantity to measure:

$$G(\varepsilon) = \frac{1}{(\varepsilon + i\delta_+)S - H}$$

Where δ_+ are an infinitesimal positive number and S, H the overlap and Hamiltonian matrices, respectively, of the entire system. The Green's function is only required for the central region and can be calculated from the Hamiltonian of the central region by adding the electrode self-energies:

$$G(\varepsilon) = [(\varepsilon + i\delta_+)S - H - \Sigma^L(\varepsilon) - \Sigma^R(\varepsilon)]^{-1}$$

The calculation of the Green's function of the central region at a specific energy, therefore basically requires the inversion of the Hamiltonian matrix of the central region.

3.2.2 The Self-Energy:

The self-energies describe the effect of the electrode states on the electronic structure of the central region. The self-energy can be calculated from the electrode Hamiltonian. ATK provides 3 different methods for calculating the self-energy:

Recursion Self Energy:

A semi-infinite matrix A_{LL} can be divided into

$$A_{LL} = \begin{bmatrix} A_{L'L'} & A_{L'0} \\ A_{0L'} & A_{00} \end{bmatrix}$$

$$g^{L}_{0,0} = \left[A_{0,0} - A_{0L'}A_{L'L'}A_{L'0}\right] = \left[A_{0,0} - A_{0,-1}g^{L'}_{-1,-1}A_{-1,0}\right]$$

$$A_{L'L'} = A_{LL} and\ g^{L}_{0,0} = g^{L'}_{-1,-1}$$

Then we obtain the matrix quadratic equation for $g^{L}_{0,0}$

$$g^{L}_{0,0} = \left[A_{0,0} - A_{0,-1}g^{L}_{0,0}A_{-1,0}\right]$$

In the same way the quadratic equation for $g^{R}_{M+1,M+1}$ can be obtained:

$$g^{R}_{M+1,M+1} = \left[A_{0,0} - A_{-1,0}g^{R}_{M+1,M+1}A_{0,-1}\right]$$

The matrix quadratic equation gives a simple iterative scheme for calculating surface green's functions. However, they must be calculated by iterating until self-consistency is achieved. This usually involves more than 50 iterations. Especially, when $g^{L}_{0,0}\ or\ g^{R}_{M+1,M+1}$ is in the neighborhood of singularities when several hundred iterations may be needed to get an accurate result.

An iterative scheme is developed which converges much faster. After n iterations 2^n unit cells instead of n unit cells are taken into account. The following series of matrix equations are obtained:

$$A_{0,0}g^{L}_{0,0} = I - A_{0,-1}g^{L}_{-1,0}$$

$$A_{-1,-1}g^L_{-1,0} = -A_{-1,0}g^L_{0,0} - A_{-1,-2}g^L_{-2,0}$$

$$A_{-2,-2}g^L_{-1,0} = A_{-2,-1}g^L_{-1,0} - A_{-2,-1}g^L_{-1,0} - A_{-2,-3}g^L_{-3,0}$$

The general term can be written as:

$$g^L_{-n,0} = A^{-1}_{0,0}\left(-A_{0,-1}g^L_{-n+1,0} - A_{0,-1}g^L_{-n-n,0}\right) = t_0 g^L_{-n+1,0} + \tilde{t_0}g^L_{-n-1,0}$$

With $t_0 = -A^{-1}_{0,0}A_{0,-1}\ and\ \ \tilde{t_0} = -A^{-1}_{0,0}A_{0,-1}$

$$g_{-n,0} = t_0\left(t_0 g^L_{-n+2,0} + \tilde{t_0}g^L_{-n,0}\right) + \tilde{t_0}(t_0 g^L_{-n,0} + \tilde{t_0}g^L_{-n-2,0})$$

$$g^L_{-n,0} = t_1 g^L_{-n+2,0} + \tilde{t_1}g^L_{-n-2,0}$$

Where

$t_1 = (I - t_0\tilde{t_0} - \tilde{t_0}t_0)^{-1}t_0^2$

$\tilde{t_1} = (I - t_0\tilde{t_0} - \tilde{t_0}t_0)^{-1}\tilde{t_0}^2$

The process can be repeated iteratively to obtain:

$$g^L_{-n,0} = t_i g^L_{-n+2^i,0} + \tilde{t_i}g^L_{-n-2^i,0}$$

The following chain of equations are obtained:

$$g^L_{-1,0} = t_0 g^L_{0,0} + \tilde{t_0}g^L_{-2,0}$$

$$g^L_{-2,0} = t_1 g^L_{0,0} + \tilde{t}_1 g^L_{-4,0}$$

$$g^L_{-2^n,0} = t_n g^L_{0,0} + \tilde{t_n} g^L_{-2^{n+1},0}$$

3.2.3 The Effective Potential:

Once the non-equilibrium density is obtained the next step in the self-consistent calculation is the calculation of the effective potential. The calculation of the exchange-correlation potential is straight forward since it is a local or semi-local function of the density.

Transmission Coefficient:

When the self-consistent non-equilibrium density matrix has been obtained, it is possible to calculate various transport properties of the system. One of the most notable is the transmission spectrum from which we can obtain the current and differential conductance.

By the transmission amplitude t_k we define the fraction of a scattering state k which propagates through a device. The transmission coefficient at energy ε is obtained by summing up the transmission from all the states at this energy. The transmission coefficient may be obtained from the retarded Green's function using:

$$T(\varepsilon) = G(\varepsilon)\Gamma^L(\varepsilon)G^\dagger(\varepsilon)\Gamma^R(\varepsilon)$$

The Electric Current:

To calculate the current we must first calculate a Transmission Spectrum. This approach has the advantage that once the transmission spectrum is calculated, it is fast to calculate the current for different electrode temperatures. The current is calculated from the transmission coefficient using:

$$I(V_L,V_R,T_L,T_R) = \frac{e}{h}\sum_\sigma \int T_\sigma(E)\,[\,f\left(\frac{E-\mu_R}{k_B T_R}\right) - f\left(\frac{E-\mu_L}{k_B T_L}\right)\,]\,dE$$

Where *f* is the Fermi function, $T_{L/R}$ is the electron temperatures of the right/left electrode and $T_\sigma(E)$ is the transmission coefficient for the spin component σ.

Differential Conductance:

The differential conductance is calculated from the transmission spectrum using:

$$\sigma(V_L,V_R,T_L,T_R,\alpha_L,\alpha_R) = \lim_{\delta V\to\infty}\left(\frac{I(V_L,\alpha_L\delta V, V_R-\alpha_R\delta V, T_L, T_R}{\delta V}\right)$$

The coupling constants $\alpha_L + \alpha_R = 1.0$ models how the transmission spectrum couples with the left and right electrode.

Chapter 4: Results and Discussion

We have analyzed the adsorption effect on semiconductive A-GNR (N=10), metallic A-GNR (N=11) and cascade hetero-GNR structure, where sensing medium is semiconducting A-GNR (N=10) which is connected to metallic A-GNR (N=11). At first, we have considered the homogenous semiconductive A-GNR (N=10) sheet as sensing medium. Then, we have analyzed transport after adsorption of two, four, six, eight and ten H_2O on that GNR sheet. Fig.3 shows the simulated I-V curves of semiconducting A-GNR. Typically the GNR sheet doesn't show significant conduction at bias voltage of below 0.75 V and then its conduction increases with the increment of bias voltage, V_b, whereas adsorption of H_2O increases the current more significantly depending on number of adsorbed water molecule.But this behaviour seems to be true before adsorbing seven water molecules on GNR sheet.

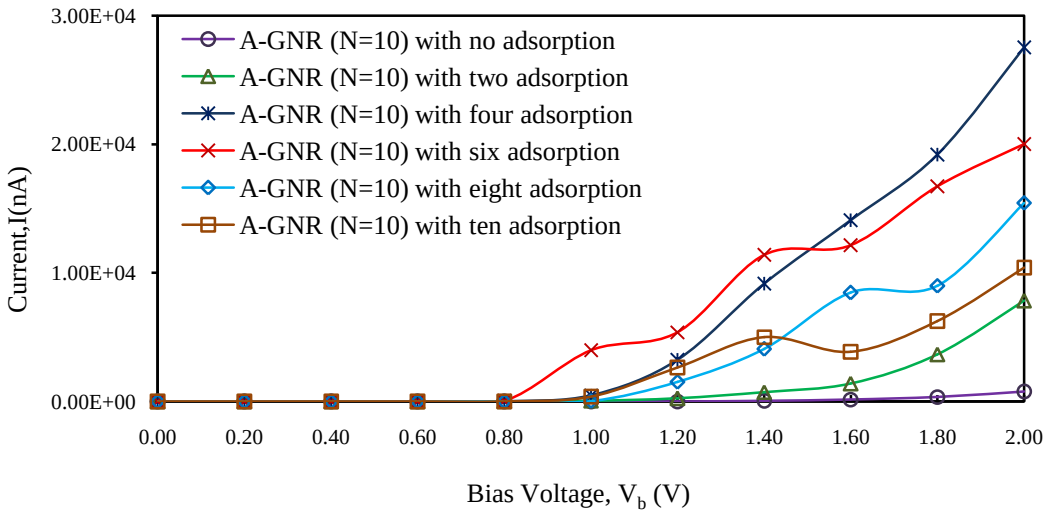

Fig. 3 I-V curves of semiconducting A-GNR (N=10) with and without H_2O adsorption

After adsorbing eight and ten H_2O molecule on GNR sheets it has been seen that the conduction of GNR decreases with the increment of bias voltage, V_b. Another important property is being observed then that due to increase number of adsorbed H_2O molecules decreases current significantly. It has been calculated that for area of semiconducting GNR, A_{GNR} of 1.1nm× 5.28 nm where the width of GNR, W_{GNR} = 1.1 nm and the length

of GNR, L_{GNR} =5.28 nm, the limitation of increasing current is to absorb not more than six H_2O molecules.

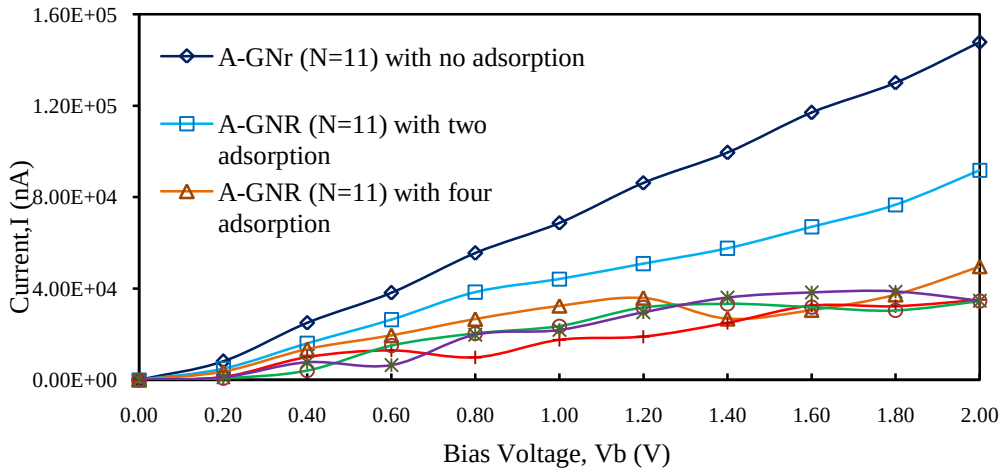

Fig. 4 I-V curves of metallic A-GNR (N=11) with and without H_2O adsorption

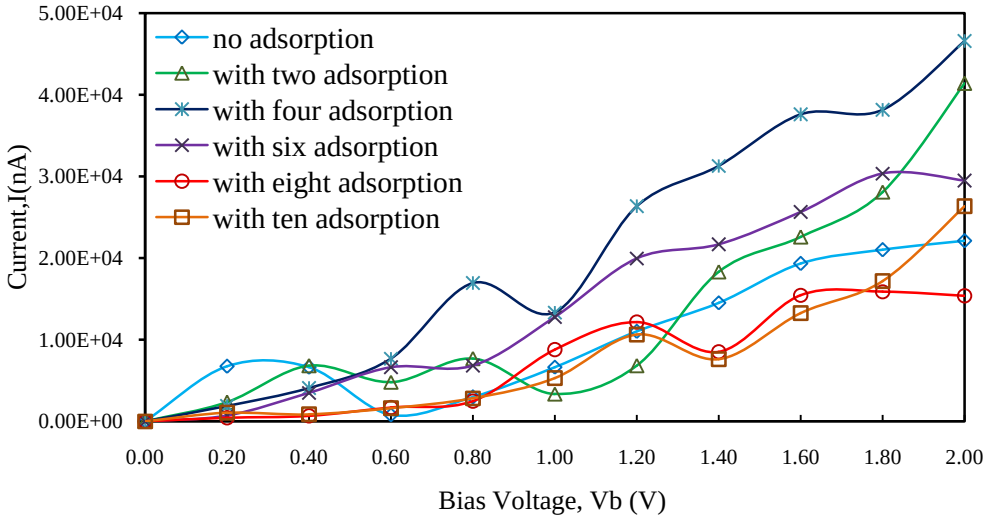

Fig. 5I-V curves of cascade Hetero-GNR used semiconducting A-GNR (N=10) as sensing medium and metallic A-GNR(N=11) as electrodes.

Fig.4 and Fig.5 shows IV curves of metallic A-GNR and cascade hetero-GNR. Here we found that the cascade structure shows significant conduction even in lower voltage (V_b=0.35V) than a homogenous semiconducting A-GNR (V_b=1V). There is a drop of current at bias voltage V_b=0.75V of cascade Hetero-GNR. It has been observed that the increment and decrement of current maintains almost a periodic cycle of cascade hetero-

GNR between 0 to 2 bias voltages. In case of metallic A-GNR is less sensible in current adsorbing H_2O molecule at low bias voltage. The conduction of metallic A-GNR decreases with the increment of bias voltage, V_b, whereas adsorption of H_2O decreases the current more significantly depending on number of adsorbed water molecule. Again, this statement is true before adsorbing seven H_2O molecules on metallic A-GNR as the increases of conductance that resulting increment of current has been found then. Due to the reverse conduction property after adsorbing seven H_2O molecules on metallic A-GNR, we have calculated the optimum area for adsorbing six water molecules without disturbing the decrement of current.

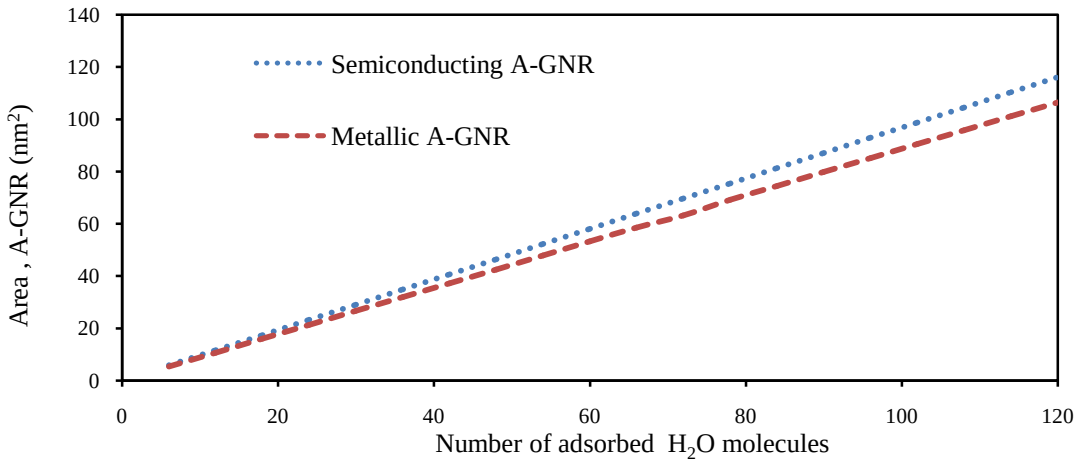

Fig. 6 Possible number of highest H_2O molecules that can be adsorbed on area of metallic A-GNR (N=11) and semiconducting A-GNR (N=10) for obtaining minimum and maximum conductivity respectively.

We have found the optimum area of adsorbing six water molecules is 1.21nm× 4.4 nm where the width of metallic A-GNR, W_{GNR} is 1.21 nm and the length of metallic A-GNR, L_{GNR} is 4.4 nm. Fig.4 illustrates the optimal area of A-GNR both of metallic and semiconducting for adsorbing maximum number of H_2O molecules on it for getting the lowest and the highest amount of conductivity respectively. Fig. 7 (a) and (b)shows that, in semiconducting GNR current increases with increased number of adsorbed H_2O molecules until the sixth H_2O molecules is adsorbed but after adsorption of eight or more molecules current significantly decreases. Fig 7 (c),(d),(e) and (f) shows the current characteristics of metallic and cascaded GNR at fixed bias voltage of 0.8V and 1.0V

respectively. It shows that with increment of adsorbed H_2O molecules current decreases at metallic GNR sheet but after adsorbing six H_2O molecules it started increasing. For cascaded GNR current shows different nature with different bias voltage, at 0.8V current increases upto four adsorption, after that it decreases sharply and for 1.0V it shows periodic nature.

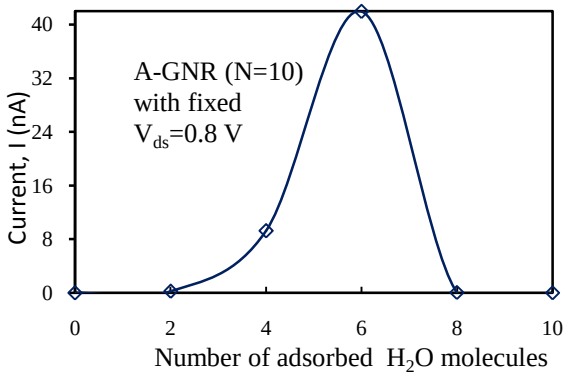

(a)

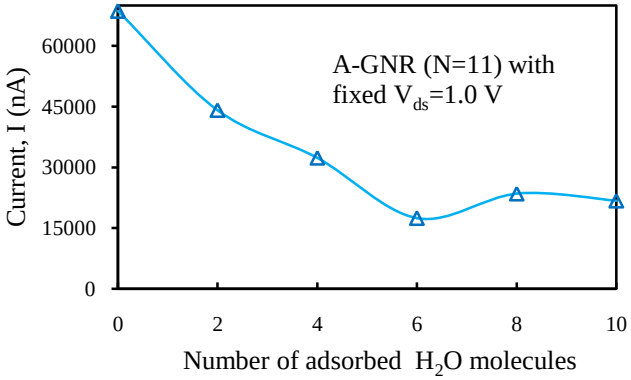

(d)

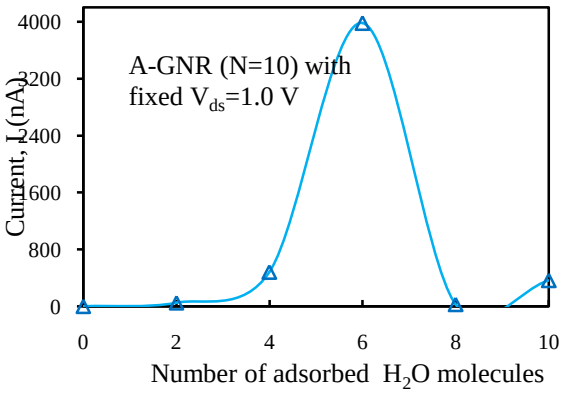

(b)

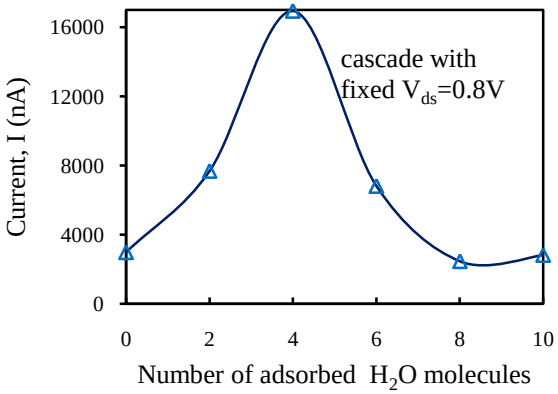

(e)

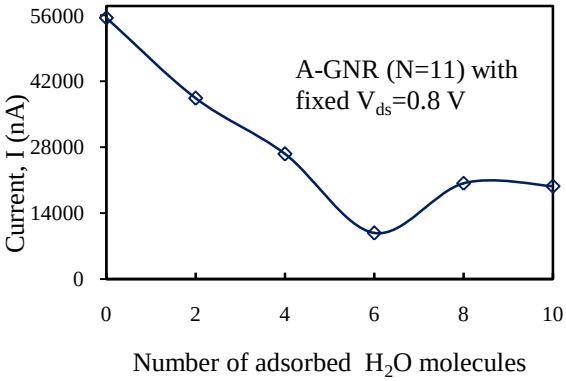

(c)

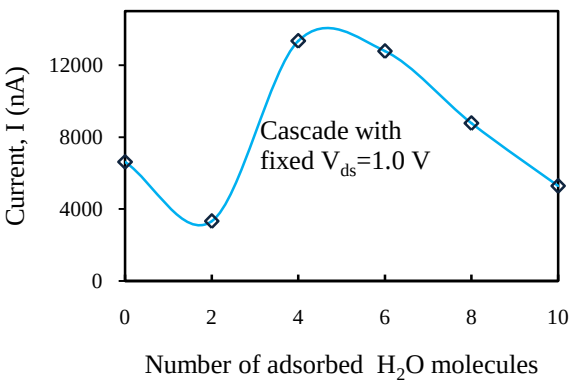

(f)

Fig. 7 Changes in current with number of adsorbed H_2O molecules in metallic A-GNR (N=11) , semiconducting A-GNR (N=10) and cascaded A-GNR .

To get described physical insight of sensing phenomenon we have to investigate the change in device density of states (DDOS), conductance (G) and electrostatic difference potential (EDP) with the amount of H_2O adsorption.Fig.8 and Fig.9 show DDOS and G respectively of a semiconducting A-GNR (N=10) for different H_2O adsorption condition. At equilibrium stage, without applying any bias voltage on semiconducting A-GNR shows Energy, E=0 signifies Fermi energy. For unadsorbed semiconducting A-GNR sheet bandgap regions contains no energy states therefore the conduction is zero within this energy range (Fig. 5(a) and Fig. 6(a)). Afterwards adsorbing of number of H_2O molecules causes suppressed of number of energy states at higher energy level, whereas some electrons become localized due to heavy nuclei of oxygen atom from H_2O molecules. The resulting effect of this electron localization is to generate some small potential barriers within the GNR sheet. These locally generated potential barriers can be seen from EDP.

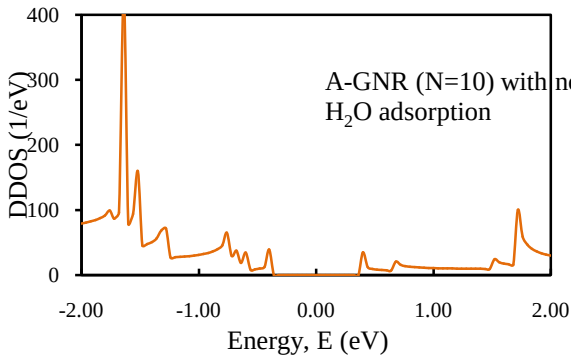

(a)

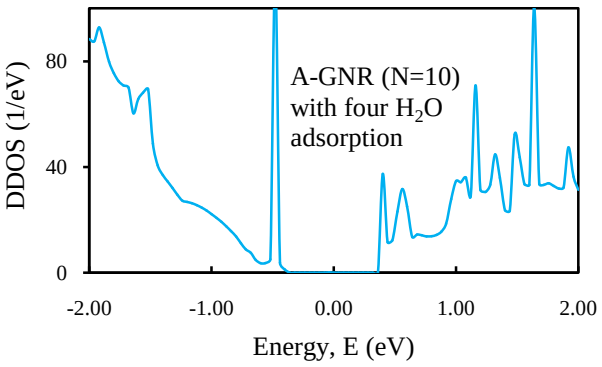

(c)

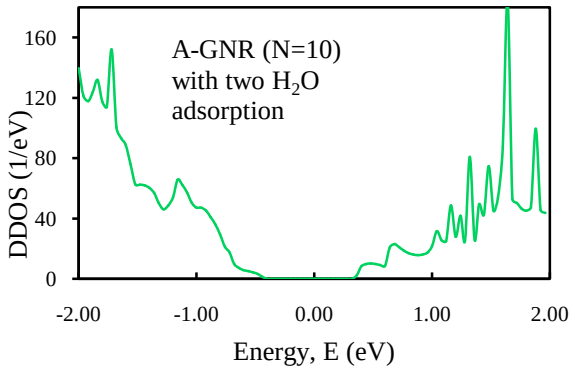

(b)

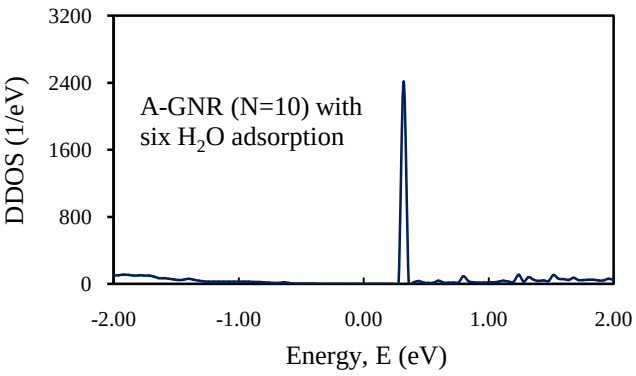

(d)

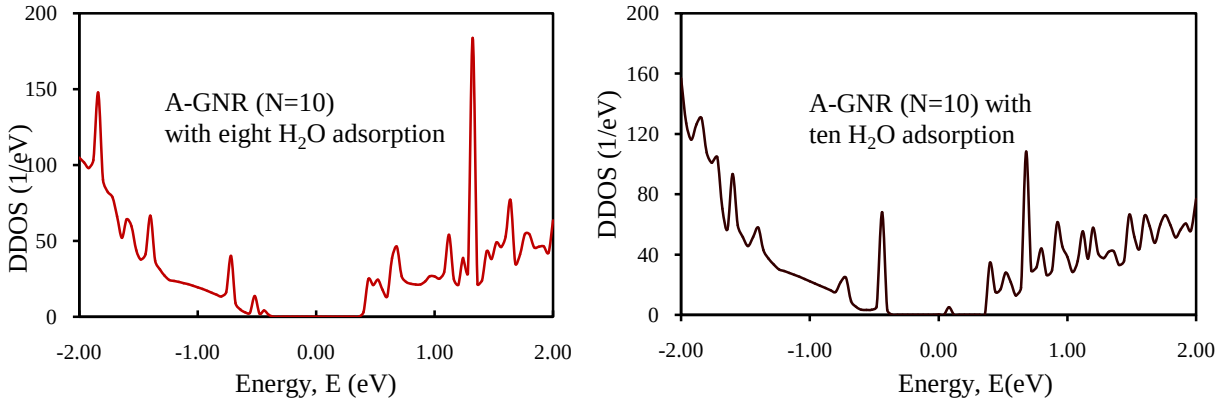

(e) (f)

Fig. 8 Device Density of States (DDOS) of semiconducting A-GNR(N=10) sheet (a) Without H_2O adsorption (b) Two H_2O adsorbed (c) Four H_2O adsorbed (d) Six H_2O adsorbed (e) Eight H_2O adsorbed (f) Ten H_2O adsorbed.

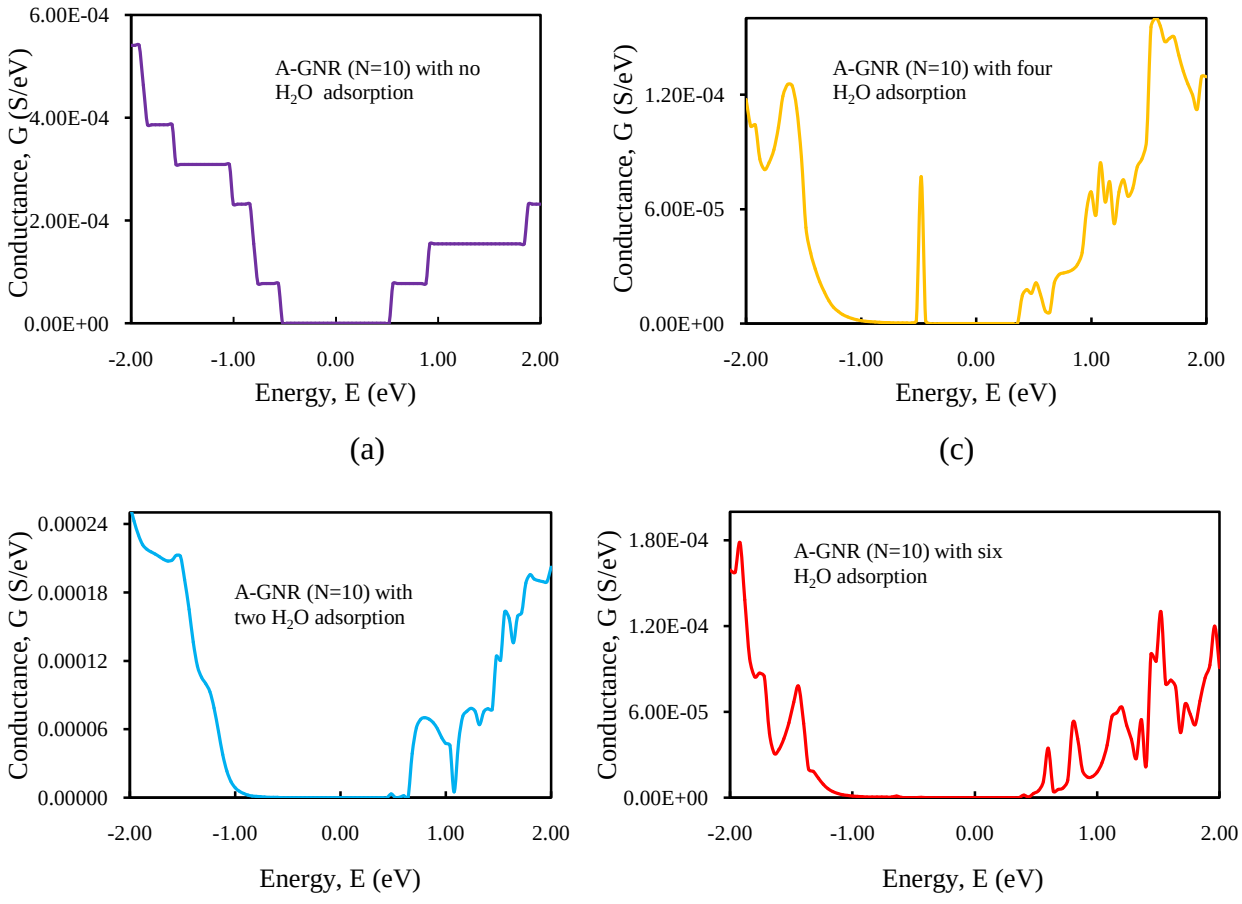

(a) (c)

(b) (d)

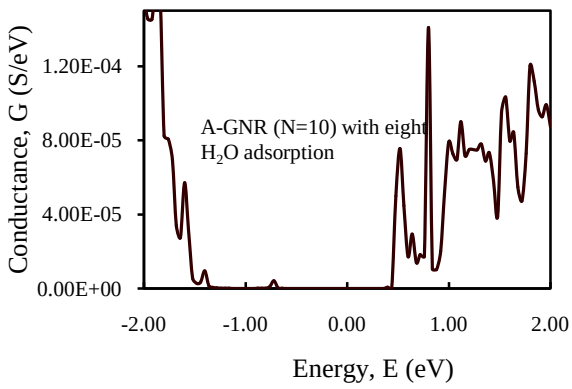

(e)

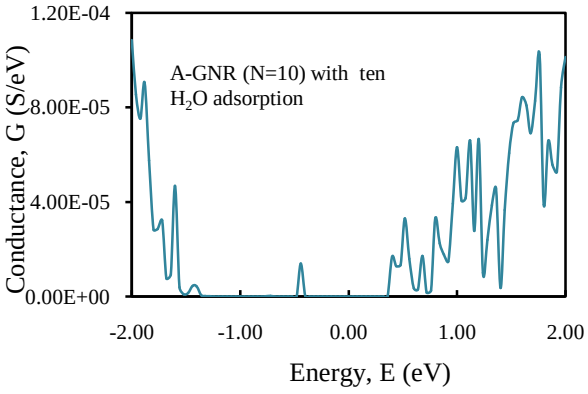

(f)

Fig. 9 Conductance of semiconducting A-GNR (N=10) sheet (a) Without H_2O adsorption (b) Two H_2O adsorbed (c) Four H_2O adsorbed (d) Six H_2O adsorbed (e) Eight H_2O adsorbed (f) Ten H_2O adsorbed.

The difference in sheet in three different direction of the A-GNR is shown in Fig.10(a). In transport direction or along the length of A-GNR potential is zero everywhere. It has been shown that with the adsoption of two H_2O molecules results two peaks in potential profile working as potential barriers for electrons. These potential barriers give rise to quasi quantizes energy states at lower energy range which is evident from Fig. 8(b). The conductance of the GNR is increased at lower energy with the help of such low energy states (Fig.9 (b)) which in turns enable significant current increment even in lower bias voltage, V_b. The number of potential barriers is increased with the increment of number of adsorbed H_2O molecules.

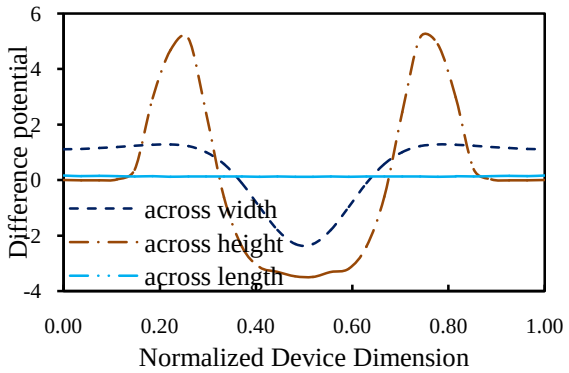

(a)

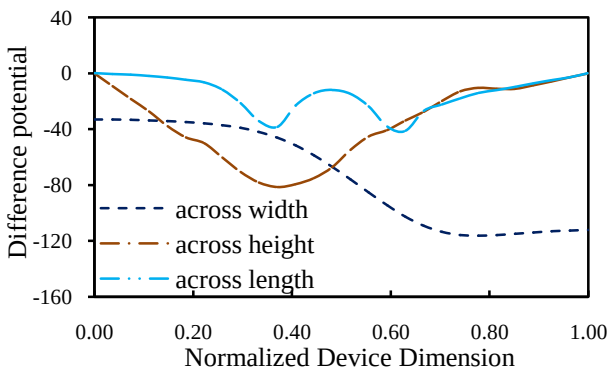

(b)

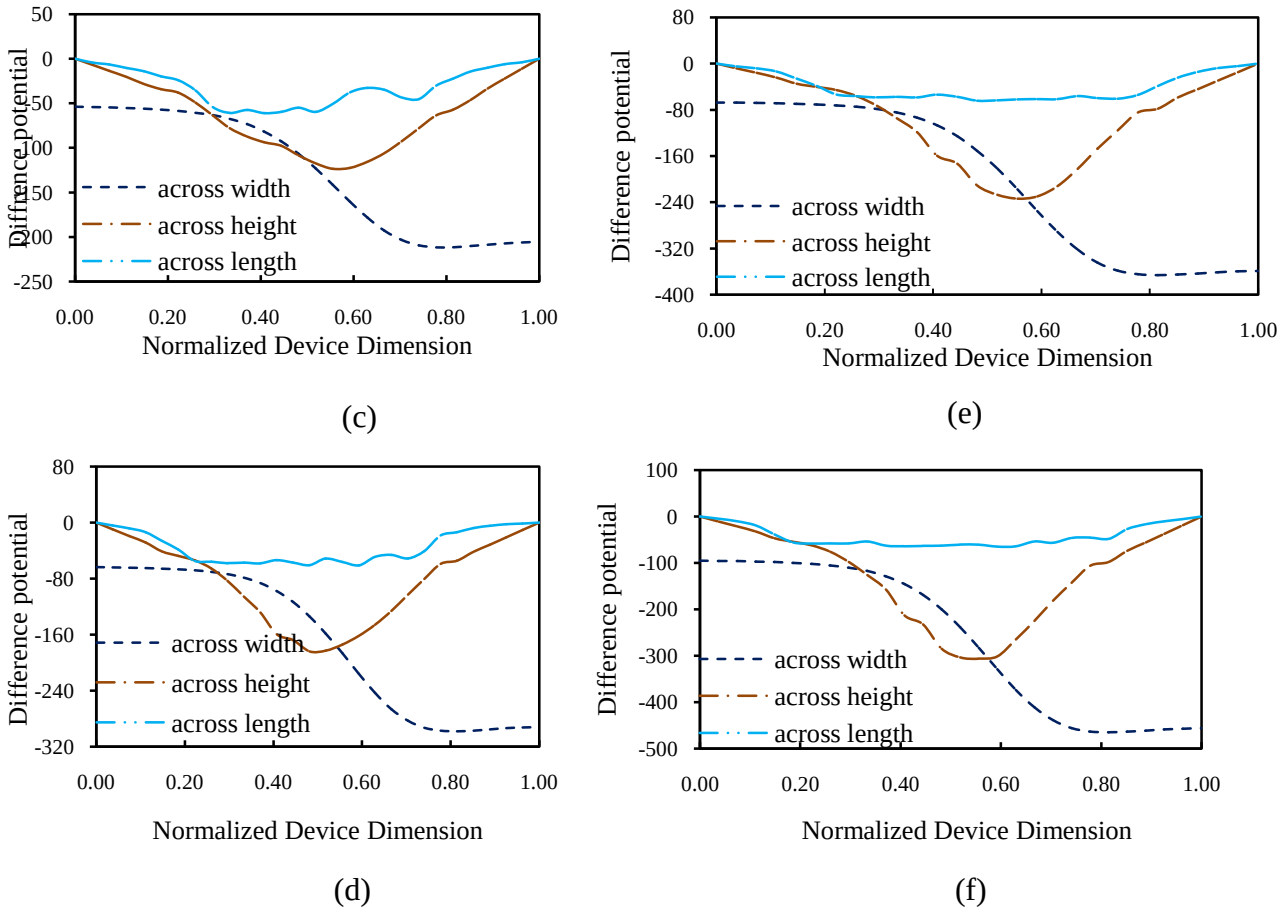

Fig. 10 Electrostatic Difference Potential (EDP) of semiconducting A-GNR (N=10) sheet (a) Without H_2O adsorption (b) Two H_2O adsorbed (c) Four H_2O adsorbed (d) Six H_2O adsorbed (e) Eight H_2O adsorbed (f) Ten H_2O adsorbed.

At Fig. (10(c) and 10(d)) there is four and six peaks in potential profile of GNR along the transmission direction because of the adsorption of four and six H_2O molecules respectively. Because of such closely packed but relatively lower height of potential barriers the ground state of quantized energy states become lower and fall within the bandgap region, which enables electronic conduction within bandgap region of the semiconducting A-GNR sheet shown at Fig.8(c), Fig.9(c), Fig.8(d) & Fig. 9(d). Therefore, insertion of such inter-bandgap electronic conduction, current starts to increase in GNR even at lower bias voltage, V_b. The energy state within bandgap region gives the highest peak and maximum number of insertion energy state within bandgap region turn maximum conductivity of semiconducting A-GNR after adsorbing six H_2O molecules that result highest amount of current which is evident from Fig.3. Again, after adsorbing of eight water molecule on A-GNR produces eight peaks in potential profile

along the length of GNR (Fig .10(e)). Due to the closely packed of potential barriers within small region prevent from making energy states between them and then act as a whole. Any electron coming to this region will experience this slop and passes this region very quickly due to the absence of inter-bandgap energy state which results the reduction of conduction area is shown in Fig. 9(e) & Fig.9 (f).

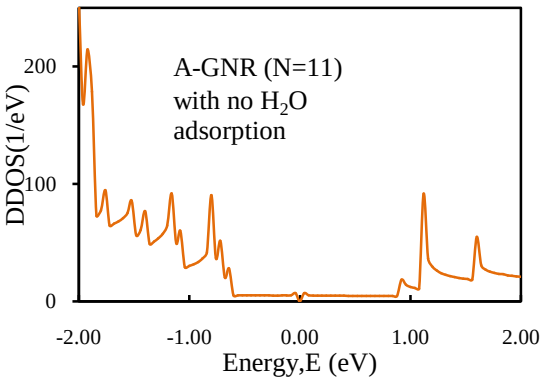

(a)

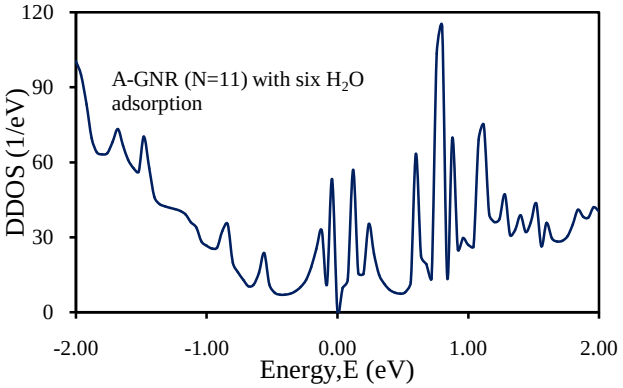

(d)

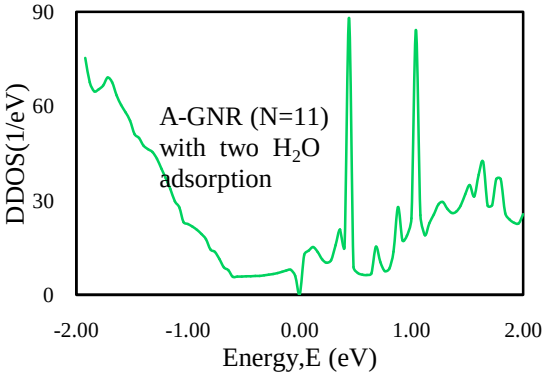

(b)

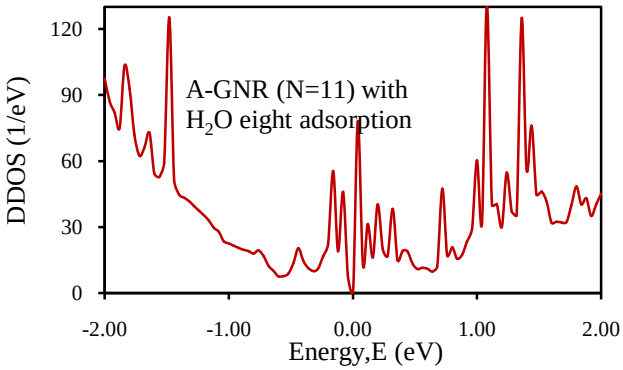

(e)

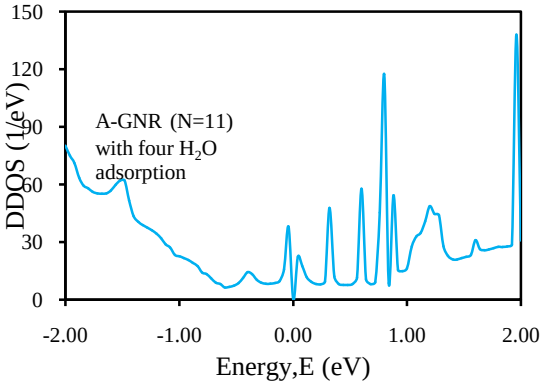

(c)

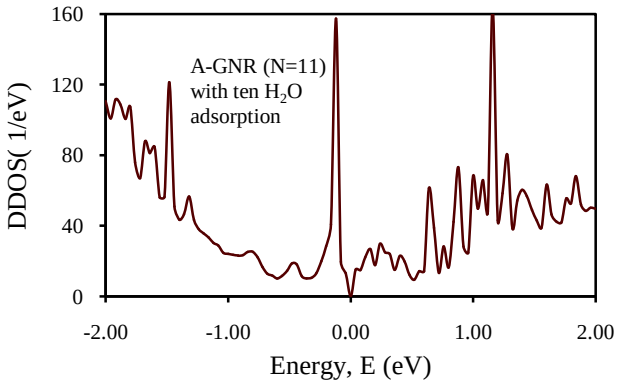

(f)

Fig.11 Device Density of States (DDOS) of metallic A-GNR(N=11) sheet (a) Without H_2O adsorption (b) Two H_2O adsorbed (c) Four H_2O adsorbed (d) Six H_2O adsorbed (e) Eight H_2O adsorbed (f) Ten H_2O adsorbed.

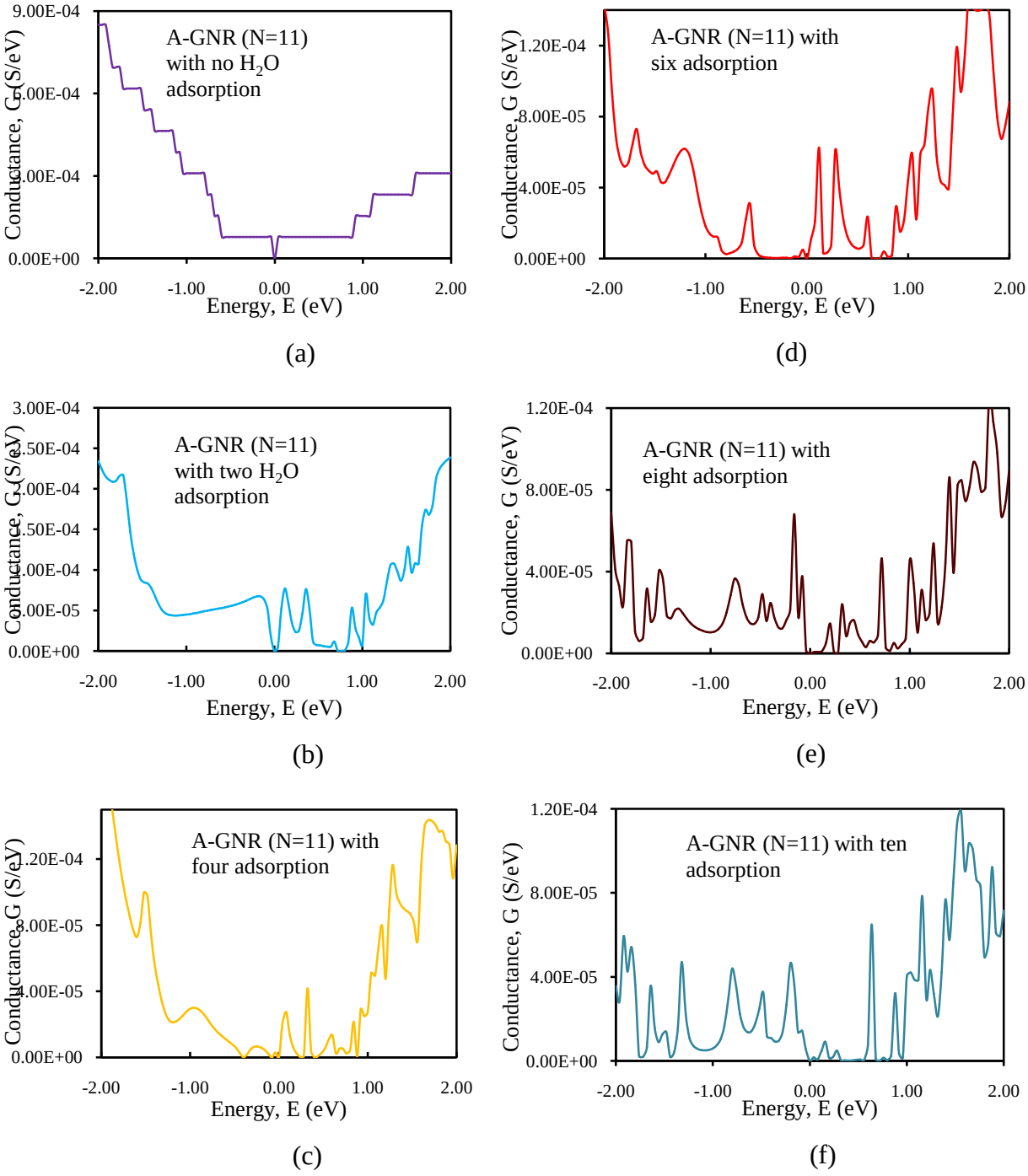

Fig. 12 Conductance of metallic A-GNR (N=11) sheet (a) Without H_2O adsorption (b) Two H_2O adsorbed (c) Four H_2O adsorbed (d) Six H_2O adsorbed (e) Eight H_2O adsorbed (f) Ten H_2O adsorbed .

The presences of only potential barriers have not made any impact towards conductivity unless fallen to the bandgap region or conduction region (Fig.8(e) & Fig.8 (f)) as a result the decrement of current has been experienced after adsorbing of eight and ten H_2O molecules on A-GNR sheet which goes to the statement of Fig.3.The DDOS and G of a metallic A-GNR (N=13) for different H2O adsorption condition is shown in Fig.11 and Fig.12. Energy, E=0 signifies Fermi energy when GNR sheet is at equilibrium. Metallic A-GNR (N=11) shows significant electronic conduction at very low energy because of the absence of bandgap (Fi. 11(a) and Fig.12 (a)).

Fig. 13(a) shows the difference in sheet potential in three different direction of the adsorption where eight numbers of peaks is created. Due to such closely packed and relatively small height potential barriers create localized energy state that can be responsible for enable of current flow at very low bias voltage, V_b. After adsorbing two and four water molecule on metallic A-GNR sheet the number of peak is distorted which is shown in Fig 13(b) and Fig.13(c) therefore the insertion of energy state cannot make any further impact for increasing current due to the decrement of conductance (Fig.11(b), Fig11(c), Fig.12(b), Fig.12(c)).

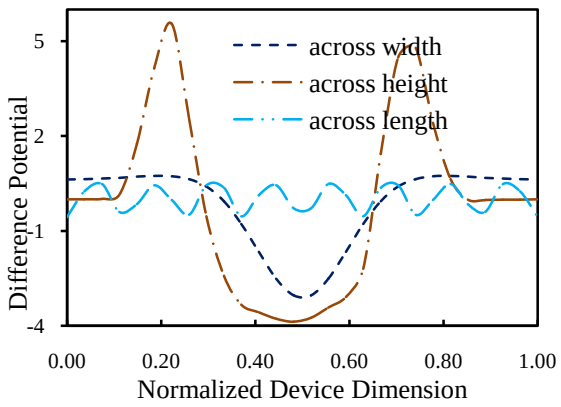

(a)

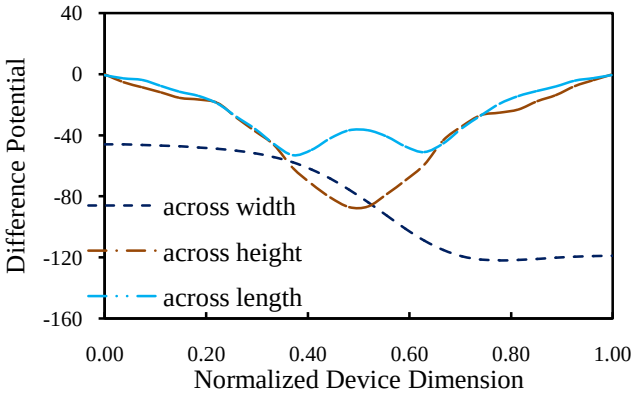

(b)

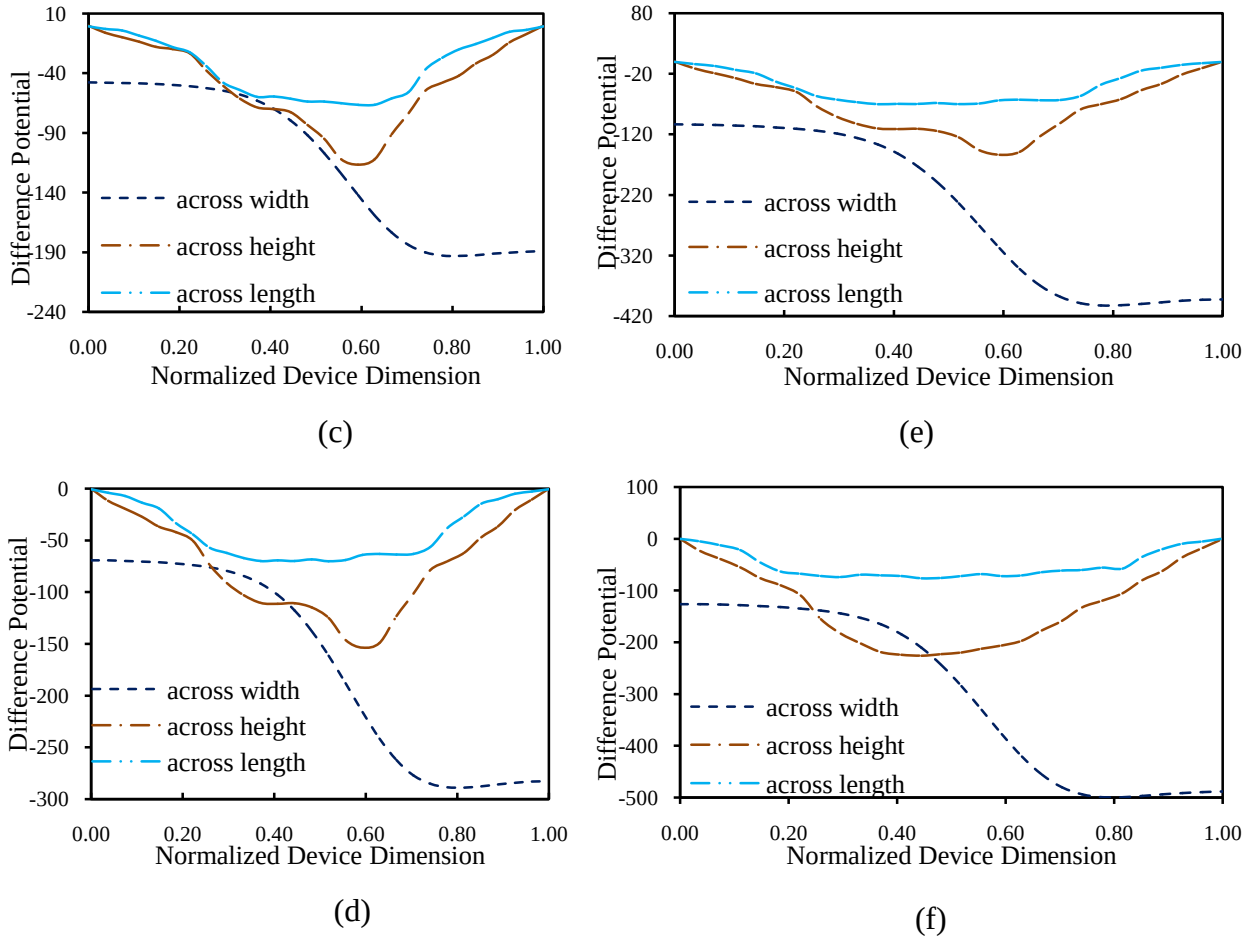

Fig. 13 Electrostatic Difference Potential (EDP) of metallic A-GNR (N=11) sheet (a) Without H_2O adsorption (b) Two H_2O adsorbed (c) Four H_2O adsorbed (d) Six H_2O adsorbed (e) Eight H_2O adsorbed (f) Ten H_2O adsorbed.

In metallic A-GNR localized states appear when there is a vacancy in their structures, and the conductance decreases due to adsorbed H_2O molecules compared with the perfect GNR. But the energy gap is not affected by the adsorbed H_2O molecule. The vacancy states are localized near the vacancy and these localized states cannot generate extra bands. The distortion of localized energy state is also disrupted after adsorbing six water molecules on metallic A-GNR resulting the reduction of conduction region (Fig.11(d),Fig.11(d) and Fig.11(e)) and therefore to decrease the current which is evident from Fig.5. the eight and ten water molecule adsorbed on metallic A-GNR resulting to produce of potential barriers relatively higher height and less compact to give an experience of passing a slope for any electron which is responsible for producing

localized energy states. Moreover, for metallic A-GNR, the conductance will be changed greatly when vacancies are putting effective channels, while remain unchanged as they are not in effective channels. It has been found that the vacancies are put in effective channel that results the increment of conduction region (Fig. 12(e) and Fig. 12(f)) and due to the insertion of localized energy states (Fig.11 (e) and Fig 11 (f)) the increment of current is found which can be seen in Fig.5.

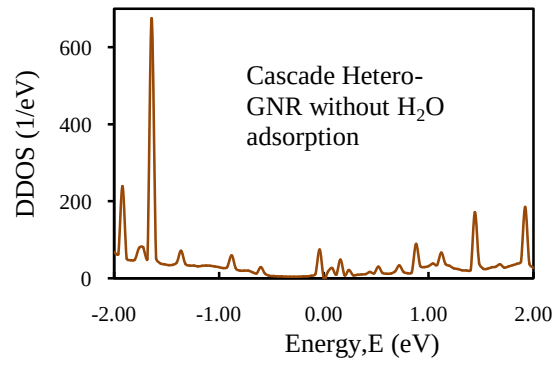

(a)

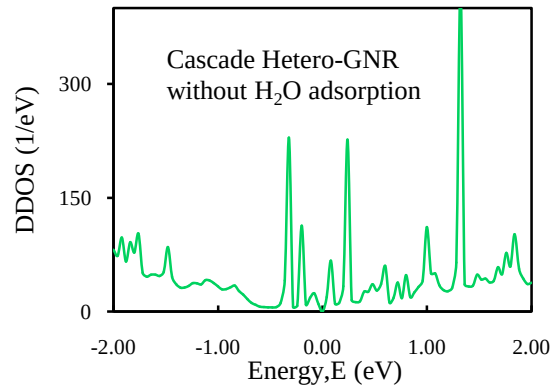

(b)

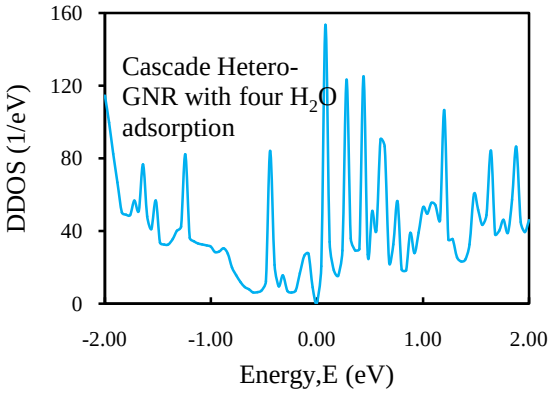

(c)

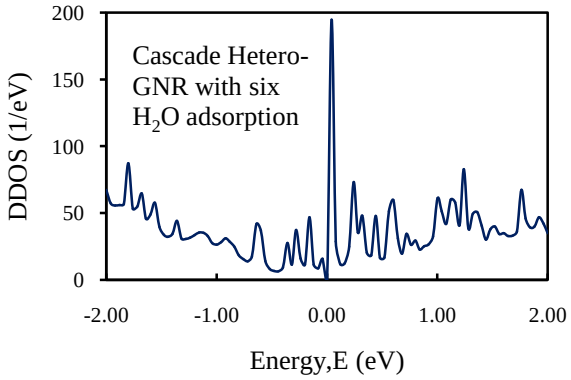

(d)

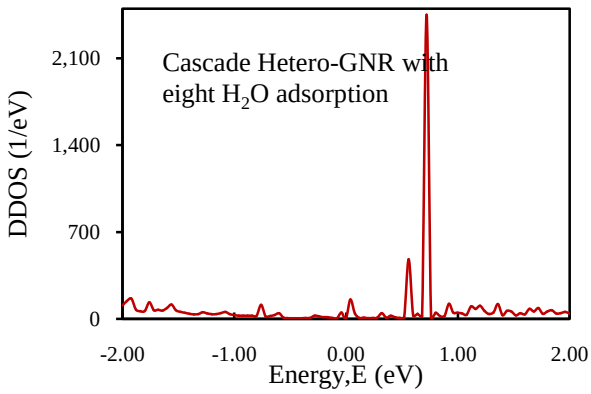

(e)

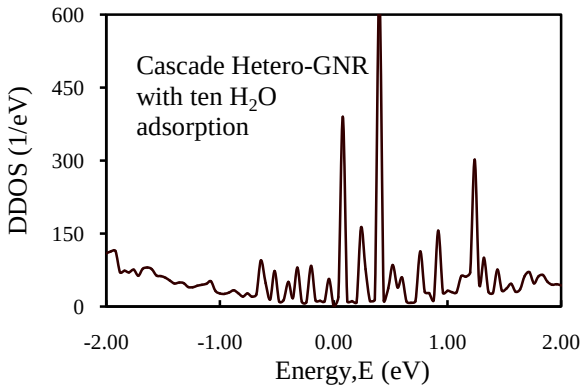

(f)

Fig. 14 Device Density of States (DDOS) of Cascade Hetero-GNR sheet (a) Without H_2O adsorption (b) Two H_2O adsorbed (c) Four H_2O adsorbed (d) Six H_2O adsorbed (e) Eight H_2O adsorbed (f) Ten H_2O adsorbed.

Cascade hetero-GNR shows significant conduction even in lower bias voltage rather than metallic A-GNR and semiconducting A-GNR. Without applying any external bias voltage, the energy, E=0 which signifies the Fermi energy. The bandgap region contains no energy state of unadsorbed cascade Hetero-GNR therefore the conduction is zero within this energy range ((Fig.14(a) and Fig.15(a)). Fig.16(a) shows the difference of sheet potential in three different direction of cascade Hetero-GNR where potential is zero along the length of GNR or in the transport direction. Due to the adsorbed two and four H_2O molecule on cascade Hetero-GNR generated two and four peaks of relatively loose and higher height in potential profile (Fig.11(b), Fig.14(c) ,Fig.15(b) and Fig. 15(c)) working as potential barriers for electrons. The quasi quantized energy states are increased with the help of these potential barriers. This low energy states are responsible for the increment of conductivity therefore increasing current. Cascade Hetero-GNR acts as semiconducting A-GNR till adsorbed four H_2O molecules. Another significant characteristic has been observed that decrement of conductance after adsorbing six, eight and ten H_2O molecules on cascade Hetero-GNR as same characteristics we have found before for metallic A-GNR. Because of increment number of adsorbed H2O molecules along transmission direction produce relatively small and flat potential barriers (Fig. 16(d), Fig. 16(e) and Fig.16(f)) therefore absence of inter-bandgap energy states resulting decrement of conductivity ((Fig.15(d),Fig.15(e) and Fig.15(f)) .

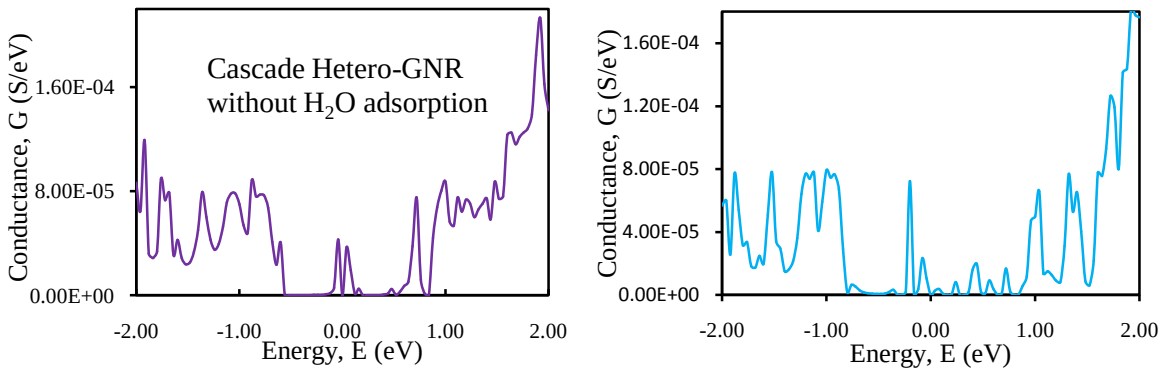

(a) (b)

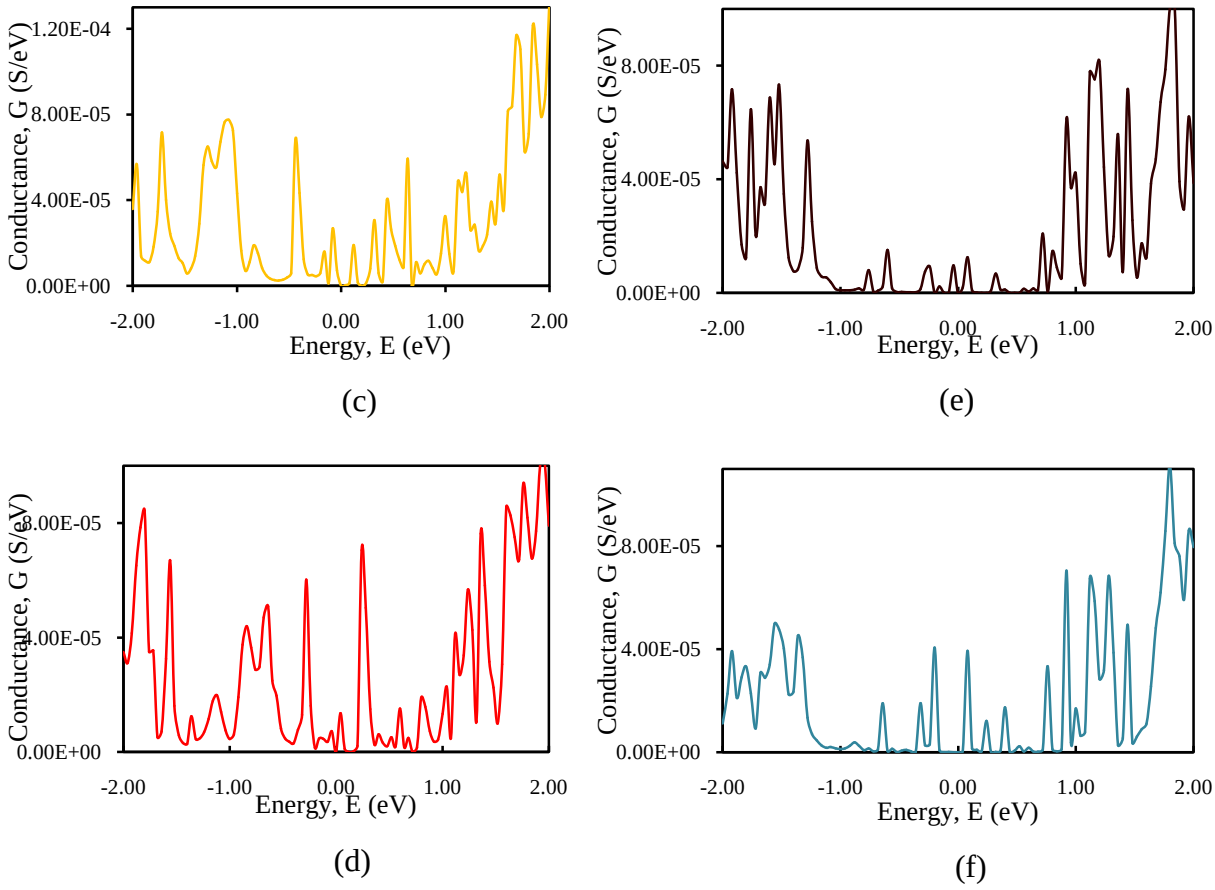

Fig. 15.Conductance of Cascade Hetero-GNR sheet (a) Without H_2O adsorption (b) Two H_2O adsorbed (c) Four H_2O adsorbed (d) Six H_2O adsorbed (e) Eight H_2O adsorbed (f) Ten H_2O adsorbed.

The increment of insertion of energy states ((Fig.14(d),Fig.14(e) and Fig.14(f)) cannot make any further impact to increase current due to the decrement of conductance .So the decrement of current after adsorbing of six, eight and ten water molecules on cascade Hetero-GNR is found which can be justified from Fig.6.

Finally we can make a statement that the adsorption process actually has two impacts on conductivity of GNR sheet. Firstly, it lowers higher energy electronic conduction of the GNRs and secondly, it enables low energy conduction through quantized energy state (even through the bandgap region of the semiconducting A-GNR. The cascade hetero-GNR can perform even at lower voltage but there might be a chance of fluctuation of result as we see in previous that it shows the characteristics of both metallic A-GNR and semiconducting A-GNR in case of adsorbed H_2O molecules. So, for a low voltage application semiconducting A-GNR will be a better choice over metallic A-GNR as the

sensing medium through metallic GNR gives higher current but less sensitive to H_2O adsorption.

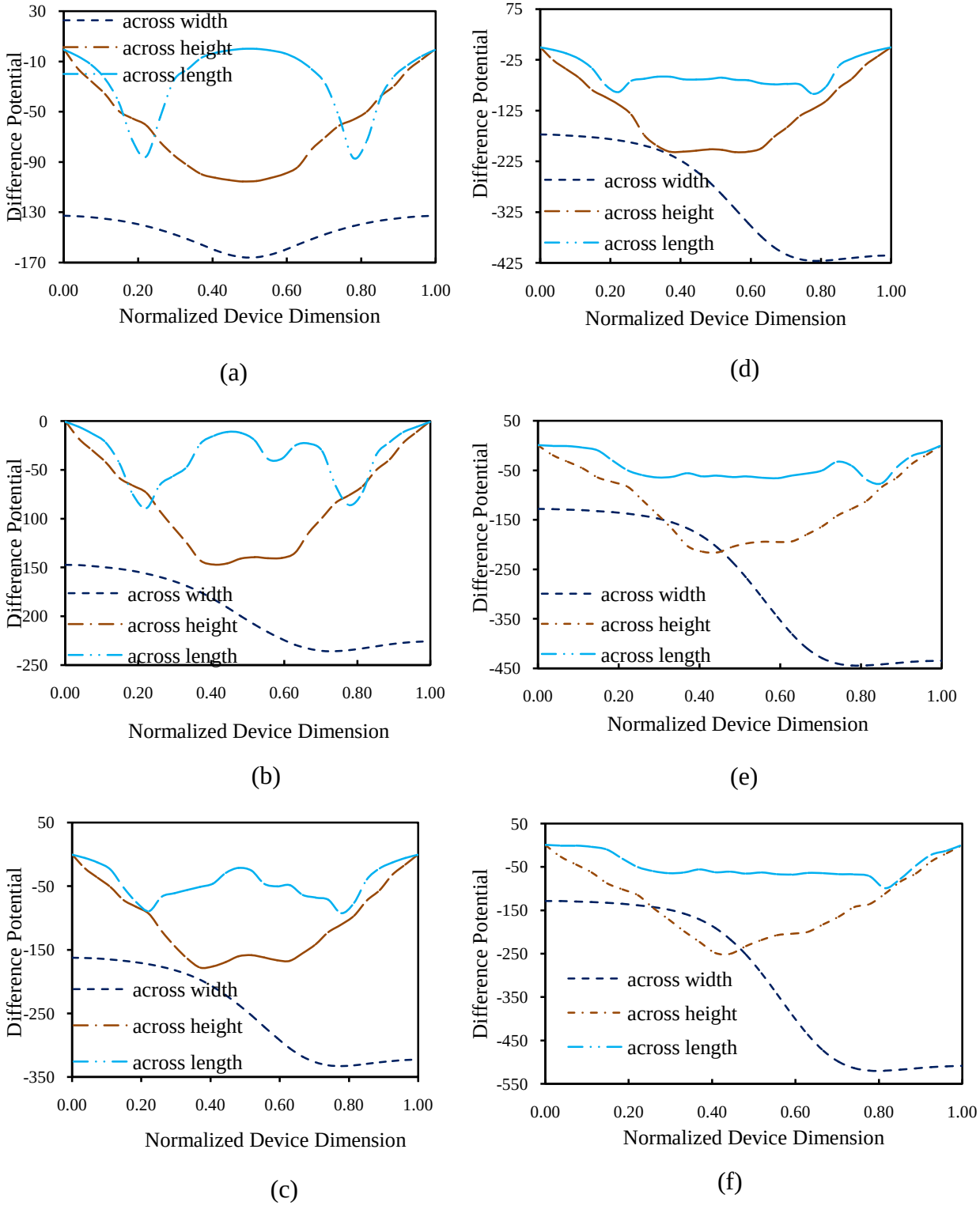

Fig. 16.Electrostatic Difference Potential (EDP) of Cascade Hetero-GNR sheet (a) Without H_2O adsorption (b) Two H_2O adsorbed (c) Four H_2O adsorbed (d) Six H_2O adsorbed (e) Eight H_2O adsorbed (f) Ten H_2O adsorbed.

Chapter 4: Conclusion:

In summary, we have investigated changes in electronic transport of A-GNR due to H_2O adsorption through self-consistent NEGF and electrostatics. Different transport properties show significant changes due to adsorption of H_2O on A-GNR surface, which become dominant in transport mechanism with increasing number of adsorbed H_2O molecules. In semiconducting A-GNR a maximum of six adsorption current increases after that current decreases with increment of adsorption. In metallic A-GNR current consistently decreases with adsorption and cascaded GNR does not show consistent behavior due to the adsorption of H_2O molecules. So increment of current in metallic A-GNR is less significant than semiconducting A-GNR with adsorption of H_2O molecules. The findings that we achieved can be very useful in developing a gas sensor and are finding a lot of practical implementations and the subject of research these days.

REFERENCE

[1]J. Berashevich and T. Chakraborty, “Tunablebandgap and magnetic ordering adsorption of molecules on graphene,” Phys. Rev. B, vol. 80, p. 033404, Jul. 2009.

[2] F. Yavari, C. Kritzinger, C. Gaire, L. Song, H. Gullapalli,T. Borca Tasciuc, P. M. Ajayan, and N. Koratkar, “TunableBandgap in Graphene by the Controlled Adsorption of Water Molecules,” Small, vol. 6, no. 22, pp. 2535–2538, Nov. 2010.

[3] B. H. Chu, C. F. Lo, J. Nicolasi, C. Y. Chang, V. Chen, W. Strupinski, S. J. Pearton, F. Ren, “Hydrogen detection using platinum coated graphene grown on SiC,” Sensor and Actuators B: Chemical, vol. 157, no. 2, pp. 500-503, Oct. 2011.

[4] K. S. Novoselov, A. K. Geim, S. V. Morozov, D. Jiang, Y. Zhang, S. V. Dubonos, I. V. Grigorieva, A. A. Firsov, “Electric Field Effect in Atomically Thin Carbon Films,” Science, Vol. 306, no. 5696, pp. 666-669, Oct. 2004.

[5] O. Leenaerts, B. Partoens, F. M. Peeters, “Adsorption of H2O, NH3, CO, NO2, and NO on graphene: A first-principles study,” Phys. Rev. B, vol. 77, no. 12, p. 125416, Mar. 2008.

[6] H. J. Yoon, D. H. Jun, J. H. Yang, Z. Zhou, S. S. Yang, M. M. C. Cheng, “Carbon dioxide gas sensor using a graphene sheet,” Sensors and Actuators B: Chemical, vol. 157, no. 1, pp. 310-313, Sep. 2011.

[7] P. R. Wallace, “The band theory of graphite,” Phys. Rev., vol. 71, pp. 622–634, 1947.

[8] Y. W. Son, M. L. Cohen, and S. G. Louie, “Energy gaps in graphene nanoribbons,” Phys. Rev. Lett., vol. 97, no. 21, p. 216803, Nov. 2006.

[9] L. Yang, C. Park, Y. Son, M. L. Cohen, and S. G. Louie, “Quasiparticle Energies and Band Gaps in GrapheneNanoribbons,” Phys. Rev. Lett., vol. 99, no. 18, p. 186801, Nov 2007.

[10] S. Datta, “Nanoscale device modeling: The Green’s function method,” SuperlatticesMicrostruct., vol. 28, no. 4, pp. 253–278, Oct. 2000.

[11] D. A. Areshkin and B. K. Nikolić, “Electron density and transport in top-gatedgraphenenanoribbon devices: First-principles Green function algorithms for systems containing a large number of atoms,” Phys. Rev.